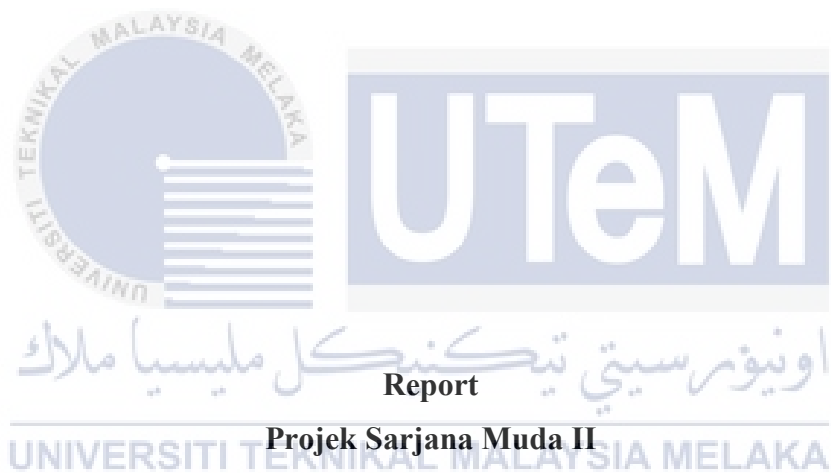


**EXPERIMENTAL STUDY ON THE EFFECT OF VORTEX
GENERATOR TO AERODYNAMICS PERFORMANCE OF
AEROFOIL**

AZUWAR BIN AZMI



Supervisor: DR. NAZRI BIN MD DAUD

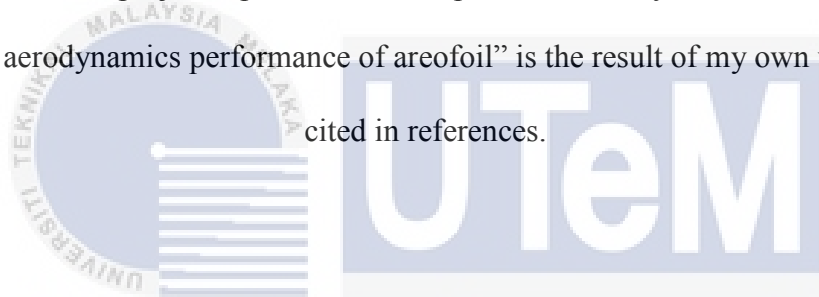
Second Examiner: DR. FADHLI BIN SYAHRIAL

**Faculty of Mechanical Engineering
Universiti Teknikal Malaysia Melaka**

MAY 2017

DECLARATION

I declare that this project report entitled “Experimental study on the effect of vortex generator to aerodynamics performance of areofoil” is the result of my own work except as cited in references.



اونيورسيتي تيكنيكل مليسيا ملاك

Signature :.....

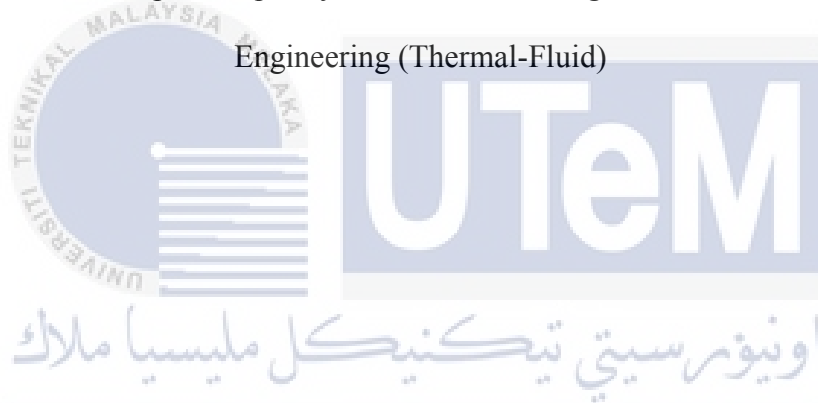
Name :...AZUWAR BIN AZMI...

Date :.....24/5/2017.....

SUPERVISOR'S DECLARATION

I hereby declare that I have read this project report and in my opinion this report is sufficient in term of scope and quality for the award of degree of Bachelor of Mechanical

Engineering (Thermal-Fluid)



Signature :

Name of Supervisor : ..DR. NAZRI BIN MD DAUD..

Date :24/5/2017.....

DEDICATION

For my beloved family members



ABSTRACT

Vortex Generator has been found to be very useful in a wide area of applications. The various types and position of vortex generator can be applied for specific tasks. For instance, the used of vortex generators have been implemented on the surface of vehicles such as BMW and on the wing of aircraft. The vortex generators used in delay the flow separation occurs toward the surface of vehicles. By applying this method, a higher amount of lift force can be obtain at the critical angle of attack apply towards an aerofoil and overcome the increasing drag force. Recently, the aerodynamics performances are frequently being studied for airflow control. The vortex generator has the ability to control airflow on wing profiles by maintaining the streamline of the boundary layer. This report attempts to define the principle and application of the vortex generator. Vortex generator is introduced in the beginning a detailed review and designs is presented. Furthermore, for the outstanding findings for this thesis are, VGs with fin shape have better aerodynamics performance compared with other cases and it achieved the functional application of VGs which are used to delay flow separation occurs on the surface of aerofoil and prevent stall at higher angle of attack applied. Last but not least this thesis had fulfil its objectives to obtain C_L and C_D for all the cases and make a comparison between the aerodynamics performances.

ABSTRAK

Penjana vorteks amatlah berguna dalam pelbagai aplikasi. Jenis-jenis dan kedudukan penjana vorteks boleh digunakan untuk tugas-tugas tertentu. Antara contoh-contoh penggunaan penjana vorteks adalah diterapkan dipermukaan kereta seperti BMW dan di bahagian sayap pesawat. Fungsi penjana vorteks ini adalah untuk melengahkan lagi pembahagian aliran bendalir di permukaan kenderaan. Dengan kaedah ini, daya angkatan dapat di naikkan pada sudut maxima yang ditujukan terhadap aerofoil serta mengatasi daya seretan dihadapi. Sejak kebelakangan ini, prestasi aerodinamik giat dikaji untuk mengawal keberkesanan prestasi aliran udara dan penjana vortex ini mempunyai kemampuan untuk mengawal aliran udara pada profil sayap dengan kaedah mengekalkan corak aliran bendalir pada lapisan sempadan (Boundary Layer). Laporan ini bertujuan mentakrifkan dasar dan aplikasi penjana vorteks. Bab dimulakan dengan introduksi kepada reka bentuk dan penerangan mendalam mengenai penjana vorteks. Sehubungan dengan itu, penemuan ketara pada tesis ini adalah penjana vorteks berbentuk sirip mempunyai kecekapan aerodinamik yg lebih tinggi berbanding kes-kes yang lain dalam kajian ini dan ia mematuhi fungsi penjana vorteks iaitu dengan menghalang pembahagian aliran pada permukaan aerofoil dan menghalang kesan “stall” berlaku pada sudut tuju yang lebih tinggi. Secara konklusinya, C_L dan C_D dapat ditentukan untuk semua kes dan perbandingan dibuat untuk setiap kajian.

ACKNOWLEDGEMENT

The heartiest appreciation goes to my project supervisor, Dr. Nazri Bin MD Daud for all his assistance, patience, guidance and valuable advice throughout the development of the project. His ideas and wisdom has helped tremendously in constructing the contents of this project. Sincerely a great appreciation indicate to Dr. Fadhli Bin Syahrial and Mr. Imran Syakir Bin Mohamad for evaluating my final year project.

I would also like to thank all the lecturers for parting knowledge as well as the staff of UTeM Mechanical Engineering Faculty in providing the help and assistance.

Last but not the least, I wish to thank all of my family members, Azmi Bin Abdul Muas, Kamilah Bt. Abdullah, Azura Bt. Azmi and Shahizatie Emilia for motivations and help. Not forgotten to all my friends for their endless support and encouragement. Again, allow me to thank you all involved in this project from the bottom of my heart.

TABLE OF CONTENTS

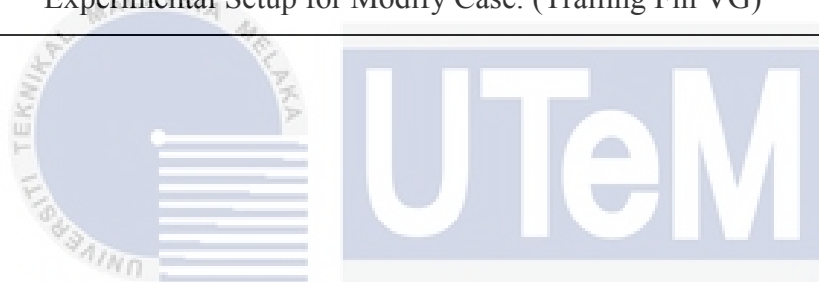
| CHAPTER | TITLE | PAGE |
|------------------|---|------|
| | DECLARATION | i |
| | SUPERVISOR’S DECLARATION | ii |
| | DEDICATION | iii |
| | ABSTRACT | iv |
| | ABSTRAK | v |
| | ACKNOWLEDGEMENT | vi |
| | TABLE OF CONTENTS | vii |
| | LIST OF TABLES | x |
| | LIST OF FIGURES | xi |
| | LIST OF SYMBOLS | xv |
| | LIST OF ABBREVIATIONS | xvii |
| CHAPTER 1 | INTRODUCTION | |
| | 1.1 Background | 1 |
| | 1.2 Problem Statement | 3 |
| | 1.3 Objective | 4 |
| | 1.4 Scope of Project | 5 |
| | 1.5 General Methodology | 6 |
| CHAPTER 2 | LITERATURE REVIEW | |
| | 2.1 Overview | 8 |
| | 2.2 Background on Vortex Generator | 9 |
| | 2.2.1 Active Vortex Generator Jets | 9 |
| | 2.2.2 Passive Vane Vortex Generators | 11 |
| | 2.2.3 Influence of Vortex Generator Vane/Fin Shapes | 13 |
| | 2.3 NACA 0015 Aerofoil | 15 |

| CHAPTER | TITTLE | PAGE |
|------------------|--|-------------|
| | 2.4 Different Flow Behaviour | 17 |
| | 2.4.1 Turbulent and Laminar Flow | 17 |
| | 2.4.2 Delay in Flow Separation | 19 |
| | 2.4.3 Stall Cells | 22 |
| | 2.4.4 Separation and Reverse Flow | 25 |
| | 2.5 Forces Exerted Towards Aerofoil | 27 |
| | 2.5.1 Pressure Distribution | 27 |
| | 2.5.2 Lift Coefficient | 29 |
| | 2.5.3 Drag Coefficient | 30 |
| | 2.6 Analysis | 31 |
| | 2.7 Discussion | 33 |
| | | |
| CHAPTER 3 | METHODOLOGY | |
| | 3.1 Introduction | 34 |
| | 3.2 Flow Chart | 36 |
| | 3.3 Experimental Equipment | 37 |
| | 3.3.1 MP 130D Subsonic Wind Tunnel, Downstream Fan | 37 |
| | 3.3.2 NACA 0015 Aerofoil | 39 |
| | 3.3.3 Vortex Generator | 40 |
| | 3.3.4 CubePro Duo 3D Printing Machine Model | 41 |
| | 3.3.5 Acrylonitrile butadiene styrene (ABS) | 42 |
| | 3.4 Design | 42 |
| | 3.4.1 Material Description and Design Drawings | 42 |
| | 3.4.1.1 NACA 0015 | 43 |
| | 3.4.1.2 Side Plat | 44 |
| | 3.4.1.3 Vortex Generators | 45 |
| | 3.4.1.4 Model Assemble | 47 |
| | 3.4.2 Design Explanation/Theory | 48 |
| | 3.4.2.1 Principle of Lift and Drag | 48 |
| | 3.5 Experimental Configuration (Measurement of Lift And Drag Force) | 50 |
| | 3.5.1 Equipment Set-up | 50 |
| | 3.5.2 Procedure of Experiment | 51 |

| CHAPTER | TITTLE | PAGE |
|------------------|--|-------------|
| CHAPTER 4 | RESULTS ANALYSIS & DISCUSSION | |
| | 4.1 Introduction | 53 |
| | 4.2 Drag Coefficients | 54 |
| | 4.3 Lift Development | 56 |
| | 4.4 Lift Coefficients | 58 |
| | 4.5 Boundary Layer | 59 |
| | 4.5.1 Boundary Layer | 59 |
| | 4.5.2 Air Velocity | 61 |
| | 4.6 Experimental Sample Calculation | 62 |
| | 4.7 Experimental Results and Analysis | 64 |
| CHAPTER 5 | RECOMMENDATION AND CONCLUSION | |
| | 5.1 Recommendation | 77 |
| | 5.2 Conclusion | 79 |
| | REFERENCES | 81 |
| | APPENDIX A: Flow Chart | 86 |
| | APPENDIX B: Gantt Chart | 87 |
| | APPENDIX C: 3D Printing Machine | 88 |

LIST OF TABLE

| FIGURE | TITLE | PAGE |
|--------|---|------|
| 4.1 | Experimental and Calculation Data to Determine C_L and C_D for Baseline Case. | 64 |
| 4.2 | Experimental and Calculation Data to Determine C_L and C_D for Modify Case. (Rectangular VG at leading edge) | 67 |
| 4.3 | Experimental and Calculation Data to Determine C_L and C_D for Modify Case. (Fin VG at leading edge) | 69 |
| 4.4 | Experimental and Calculation Data to Determine C_L and C_D for Modify Case. (Rectangular VG at trailing edge) | 72 |
| 4.5 | Experimental Setup for Modify Case. (Trailing Fin VG) | 74 |



اونيورسيتي تيكنيكل مليسيا ملاك

UNIVERSITI TEKNIKAL MALAYSIA MELAKA

LIST OF FIGURE

| FIGURE | TITLE | PAGE |
|--------|--|------|
| 1.1(a) | Rough Setup of Vortex Generator on Aerofoil. (https://www.researchgate.net/figure/283504299_fig1_Figure-1-contra-rotating-vortex-generator-configuration) | 3 |
| 1.1(b) | Vortex Generator Installment After and Before with Different Angle of Attack. (http://www.vortex-generators.com/vortex-generators.html) | 4 |
| 1.2 | Flow chart of the methodology. | 7 |
| 2.01 | The VGJ actuator geometry and parameters, also showing the additional symmetry parameters d and D for pair and array configurations. (http://fluidsengineering.asmedigitalcollection.asme.org/article.aspx?articleid=1430651) | 10 |
| 2.02 | Deployed flaps and spoilers uncover VGs close to the leading edge on a flap during landing. (https://en.wikipedia.org/wiki/Spoiler_(aeronautics)) | 11 |
| 2.03 | Types and notation of Pearcey's VVGs. Reference [Pearcey (1961)] | 12 |
| 2.04 | VVG setups and the notation: (a) counter-rotating common flow downward, and (b) co-rotating ($d = 0$) configurations. Reference [Pearcey (1961)] | 13 |
| 2.05 | Geometries of Vortex Generators and Test Conditions. (Ho-Joon Shim, Ki-Jung Kwon, and Seung-O Park, 2017) | 14 |
| 2.06 | Mean streamwise velocity contours ($h/\delta = 1.0$, $l/h = 5$, and $\alpha = 10$ deg.) (Ho-Joon Shim, Ki-Jung Kwon, and Seung-O Park, 2017) | 14 |
| 2.07 | Experimental and Numerical Results. (İzzet Şahin and Adem Acir, 2015) | 16 |
| 2.08 | Distribution of Turbulence and b) Distribution of Pressure. (İzzet Şahin and Adem Acir, 2015) | 17 |
| 2.09 | Turbulent and Laminar Boundary Flow. (Aman Sharma, 2012) | 18 |

| | | |
|------|--|----|
| 2.10 | (a) Co-rotating Vortex Generator Configuration (b) Counter-rotating Vortex Generators Configurations [Reference: (Godard and Stanislas, 2006)]. | 20 |
| 2.11 | Visual of Swirl Vortex Pattern on the Leading Edge Upper Surface [Reference: (Thompson, 1997)]. | 21 |
| 2.12 | Leading edge serrations [Reference : (Soderman, 1972)] | 21 |
| 2.13 | Plan in schematic view of the test set-up displaying the wing, the barriers, the pressure taps at the centre of the wing span, the stabilising disturbance and the Stereo PIV cameras along with the measurement planes at $x/c = 0.6$ (plane A), $x/c = 0.7$ (plane B) and $x/c = 0.8$ (plane C). The camera contained angle (ϕ) for plane C is also indicated. [Reference : (Marinos Manolesos and Spyros G.Voutsinas, 2015)] | 22 |
| 2.14 | Pressure distribution along the wind chord for a wing with and without VGs at $\alpha = 10^\circ$. [Reference : (Marinos Manolesos and Spyros G.Voutsinas, 2015)] | 23 |
| 2.15 | Experimental lift coefficient polar for a wing with and without VGs. [Reference : (Marinos Manolesos and Spyros G.Voutsinas, 2015)] | 24 |
| 2.16 | Experimental drag coefficient polar for a wing with and without VGs. [Reference : (Marinos Manolesos and Spyros G.Voutsinas, 2015)] | 24 |
| 2.17 | Qualitative Representation of Separation Types (Corten, 2001) | 25 |
| 2.18 | Coefficient Pressure Distribution over an Aerofoil (Dr. J. M. Meyers, Dr. D. G. Fletcher and Dr. Y. Dubief) | 28 |
| 3.1 | Flow Chart of the Methodology | 36 |
| 3.2 | Front View of MP 130D Subsonic Wind Tunnel. | 38 |
| 3.3 | The motor for MP 130D Subsonic Wind Tunnel. | 38 |
| 3.4 | Speed Control Module and Indicator Module. | 39 |
| 3.5 | Wind Velocity, Test Section. | 39 |
| 3.6 | Figure 3.6: NACA 0015 with labels. (https://www.researchgate.net/figure/267210609_fig1_Figure-1-NACA-0015) | 40 |
| 3.7 | Fin and Rectangular Shaped of Vortex Generator. | 40 |
| 3.8 | CubePro Duo 3D Printing Machine Model. | 41 |
| 3.9 | Acrylonitrile butadiene styrene (ABS) with the mass of 1 kg and diameter 1.76 mm. | 42 |
| 3.10 | NACA 0015, Surface Area = 13 cm x 13 cm | 43 |
| 3.11 | 2D Sketch of Side Plat. | 44 |

| | | |
|------|--|----|
| 3.12 | 3D Views of the Side Plats. | 44 |
| 3.13 | 2D Sketch for the Rectangular Shaped Vortex Generator | 45 |
| 3.14 | 3D Sketch Views of the Rectangular Shaped Vortex Generator | 45 |
| 3.15 | 2D Sketch for the Fin Shaped Vortex Generator | 46 |
| 3.16 | 3D Sketch for the Fin Shaped Vortex Generator | 46 |
| 3.17 | Assembly of Vortex Generator Experiment (Fin) | 47 |
| 3.18 | 3D Views of the Experimental Assembly (Rectangular) | 47 |
| 3.19 | Drag and Lift Forces. (Yunus A.Cengel and John M.Cimbala, 2014) | 48 |
| 3.20 | Measurement of drag and lift forces against angle of attack at various wind velocity. | 51 |
| 3.21 | Procedure for Testing Lift and Drag Force. | 52 |
| 3.22 | Experiment Setup for Baseline Case. | 52 |
| 4.01 | Figure 4.01: Drag Coefficients for Sphere and Circular Disk. (http://www.aerospaceweb.org/question/aerodynamics/q0231.shtml) | 54 |
| 4.02 | Difference of Lift to Drag Ratio with Angle of Attack for a Two Dimensional Aerofoil. (Yunus A.Cengel & John M.Cimbala, 2014) | 55 |
| 4.03 | Drag Coefficients for Flat Plate of Finite Length Normal to Flow. (https://www.slideshare.net/manrajpal/bl-concept) | 55 |
| 4.04 | Drag Coefficient Plotted against Angle of Attack for N.A.C.A Aerofoil 23015. (Yunus A.Cengel & John M.Cimbala, 2014) | 55 |
| 4.05 | Notation of a Lifting Vane (https://www.skybrary.aero/index.php/Angle_of_Attack) | 56 |
| 4.06 | Two-dimensional Flow around a Lifting Vane (http://www.pilotwings.org/airfoil-pressures.html) | 57 |
| 4.07 | Figure 4.07: Pressure Distribution for an Aerofoil (http://www.scrigroup.com/limba/engleza/114/Pressure-Distribution-on-an-Ae75232.php) | 58 |
| 4.08 | Lift and Drag Coefficients against Angle of Attacks for an Airfoil (http://flyacro.us/spintraining.html) | 59 |
| 4.09 | Air Velocity at Boundary. (https://www.comsol.com/blogs/which-turbulence-model-should-choose-cfd-application/) | 60 |
| 4.10 | Experimental Setup for Baseline Case. | 64 |
| 4.11 | Lift and Drag Coefficient Results against Angle of Attack. (Baseline Case) | 65 |

| | | |
|------|--|----|
| 4.12 | Lift and Drag Coefficient Ratio against Angle of Attack. (Baseline Case) | 65 |
| 4.13 | Experimental Setup for Modify Case. (Leading Rectangular VG) | 67 |
| 4.14 | Lift and Drag Coefficient Results against Angle of Attack. (Leading Rectangular VG) | 68 |
| 4.15 | Lift and Drag Coefficient Ratio against Angle of Attack. (Leading Rectangular VG) | 68 |
| 4.16 | Experimental Setup for Modify Case. (Leading Fin VG) | 70 |
| 4.17 | Lift and Drag Coefficient Results against Angle of Attack. (Leading Fin VG) | 70 |
| 4.18 | Lift and Drag Coefficient Ratio against Angle of Attack. (Leading Fin VG) | 70 |
| 4.19 | Experimental Setup for Modify Case. (Trailing Rectangular VG) | 72 |
| 4.20 | Lift and Drag Coefficient Results against Angle of Attack. (Trailing Rectangular VG) | 73 |
| 4.21 | Lift and Drag Coefficient Ratio against Angle of Attack. (Trailing Rectangular VG) | 73 |
| 4.22 | Experimental Setup for Modify Case. (Trailing Fin VG) | 75 |
| 4.23 | Lift and Drag Coefficient Results against Angle of Attack. (Trailing Fin VG) | 75 |
| 4.24 | Lift and Drag Coefficient Ratio against Angle of Attack. (Trailing Fin VG) | 75 |

LIST OF SYMBOL

| | |
|------------|--|
| C_D | Coefficient of Drag |
| C_L | Coefficient of Lift |
| β | Skew Angle (Degree $^\circ$) |
| α | Pitch Angle/Angle of Attack (Degree $^\circ$) |
| D | Distance Link Adjacent |
| d | Distance Between Tow |
| c^l | Chord |
| h | Height |
| δ | Boundary Layer Thickness |
| Re | Reynolds Number |
| l | Chord Length (m) |
| C_p/P | Coefficient Pressure Distribution |
| ρ | Density (kg/m 3) |
| U_{stag} | Stagnation Point |
| L | Lift Force (N) |
| v | Velocity (m/s) |
| A | Frontal Area (m 2) |
| D | Drag Force (N) |
| m | Metre |
| s | Second |
| W | Watt |
| V | Volt |
| Hz | Hertz |
| lPh | Liquid Pound per Hour |
| A | Ampere |
| μ | Dynamic Viscosity [kg/(s.m)] |
| c | Symmetrical Chord of Length |

| | |
|------------|---|
| θ | Angle |
| p_o | Pressure at Some Distance Upstream from the Section |
| p | Pressure at Any Point on the Vane Surface |
| ΔP | Dynamic pressure or P_{dyn} (N/m^2) |
| N | Weight ($kg \times \frac{m}{s^2}$) |
| X_A | Actual Distance |
| X_S | Standard Distance |
| L_o | Indicated Lift |
| D_o | Indicated Drag |
| T | Temperature ($^{\circ}C$) |
| % | Percentage |



اونيورسيتي تيكنيكل مليسيا ملاك

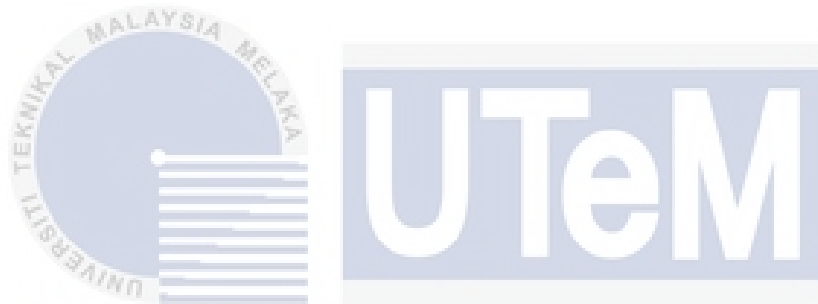
UNIVERSITI TEKNIKAL MALAYSIA MELAKA

LIST OF ABBEREVATIONS

| | |
|------------|---|
| VGs | Vortex Generators |
| VGJs | Vortex Generator Jets |
| VVGs | Vane Vortex Generators |
| UVGJ | Velocity Vortex Generator Jets |
| Φ VGJ | Exit Diameter Vortex Generator Jet |
| CFD | Computational Fluid Dynamics |
| PIV | Particle Image Velocimetry |
| NACA | National Advisory Committee for Aeronautics |
| AR | Aspect Ratio |
| T.I | Turbulence Intensity |
| SC | Stall Cell |
| ZZ | Zigzag |
| VAWT | Vertical Axis Wind Tunnel |
| 3D | Three Dimension |
| STL | STereoLithography |
| PLA | PolyLactic Acid |
| PVA | Polyvinyl alcohol |
| ABS | Acrylonitrile butadiene styrene |
| 2D | Two Dimension |
| etc | et cetera |
| DBD | Dielectric Barrier Discharge |

CHAPTER 1

INTRODUCTION



1.1 Background

Generally, vortex generator is a small angled vane in any kind of shapes and dimensions that being installed on an outer surface of an aerodynamic body. For this case of study, small angled vane with shapes of square and fin is being install on the surface on an aerofoil. The specific position for this investigation is focus on the leading edge and trailing edge of an aerofoil. The experimental test conducted in a vertical axis wind tunnel with specific parameter of air velocity supply and tilt angle of the aerofoil. Continuously related about the vortex generator, the angle of the vane will causes the air to swirl, generating a vortex behind it. This result allow the air flow to stay "attached" to the surface even at points where the flow without a vortex would separate from the surface.

One of the most common uses of vortex generators is on aircraft wings forward of an ailerons. When the aircraft wing stalls, the flow detaches from the wings. This means that the flow will detach before it reaches the ailerons, making them ineffective. The use of vortex generators helps the ailerons to provide control even if the rest of the wing is stalled.

Related with the earlier explanation, vortex generator is normally taking the shape of a vane and also influence by the size and angle of position and it generate a small vortex. This vortex is essentially a region where the flow is rotating around its axis. Basically this plate extracts energy from the flow generating this rotation on the flow.

Next, the rotational flow has gain the energy and accurately oriented interacts with the boundary layer over the wing, it can provide higher energy towards it. With the extra energy gain, it cause the boundary layer become unaffected to separation. Due to the phenomena, angle of attack can be increase and higher lift coefficient can be obtain for the aerofoil that being installed with vortex generator.

Furthermore, vortex generator will increase the amount of drag force due to oppose motion against the air and higher angle of attack. According to (Masaru Koike, Tsunehisa Nagayoshi and Naoki Hamamoto, 2004), by installing vortex generator, it can help in reducing the drag force by preventing flow separation at downstream besides delay flow separation.

At certain point, the aerofoil reaches a condition of stalling effect, both the pressure distribution on the bottom and top surface of the aerofoil is equivalent. This effect happens because of the critical angle of attack of the aerofoil is exceed.

1.2 Problem Statement

- Since, there is a lack of study in comparing baseline case and modify case (vortex generator) of aerofoil.
- To determine coefficient of drag (C_D) and lift (C_L) for baseline case and modify (vortex generator) case.
- Compare the C_D and C_L Of the modify case at the leading and trailing edge of the aerofoil.

For the vortex generator investigation, it is important to get precise configuration of apparatus and materials to determine an accurate reading of data as shown as Figure 1.1(a). The main problem in this case is to determine and study about the drag and lift coefficient of the baseline case and modify case of an aerofoil (NACA 0015). The optimum position/distance (x) of vortex generator need to be determine on the leading and trailing edge to achieve the maximum efficiency of the C_D and C_L . This method can be apply to study the aerodynamic air flow of aerofoil or vehicle. The experiment conducted in a wind tunnel with by supplying specific parameter of air velocity towards the aerofoil. Figure 1.1(b) shows and indicates the pattern of airflow before and after installing the vortex generator on the surface of an aerofoil with three different angles of attack.

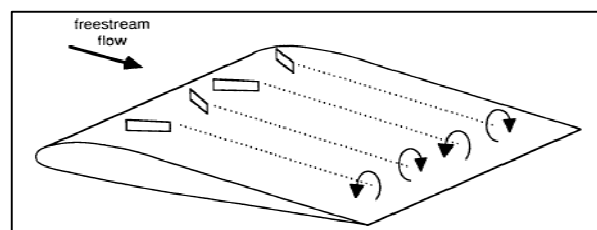


Figure 1.1(a): Rough Setup of Vortex Generator on Aerofoil.
 (https://www.researchgate.net/figure/283504299_fig1_Figure-1-contra-rotating-vortex-generator-configuration)

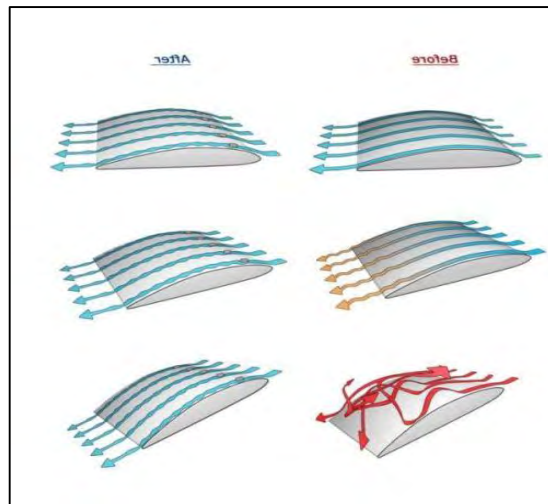
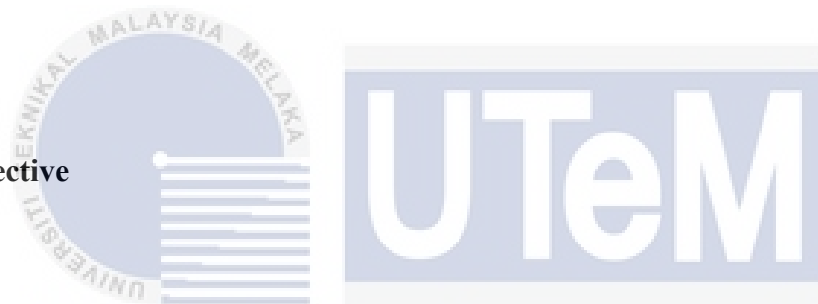


Figure 1.1(b): Vortex Generator Installment After and Before with Different Angle of Attack. (<http://www.vortex-generators.com/vortex-generators.html>)

1.3 Objective



The objectives of this project are as follows:

اونيورسيتي تيكنيكل ماليزيا ملوك
UNIVERSITI TEKNIKAL MALAYSIA MELAKA

1. To determine the C_D and C_L for the baseline case of aerofoil.
2. To determine the C_D and C_L for the modify case of aerofoil by installing vortex generator.
3. Compare both C_D and C_L for the base and modify case of aerofoil.

1.4 Scope of Project

The actions that need to be carried out to achieve the objectives in this project are listed below.

The scope for this project are:

1. Type of aerofoil being use:
2. Fix air velocity measurement:
3. Measure C_D and C_L .

Only vortex generator findings are presented in this report. The result of the airflow, C_D and C_L can be obtained during the experiment conduct with the helps from technician and supervisor.

In order to manipulate C_D and C_L , these three main fields of flow control can be investigated:

- a) Angle of attack of the aerofoil.
- b) Position of the vortex generator being install.
- c) Shape of the vortex generator.

1.5 General Methodology

The actions that need to be carried out to achieve the objectives in this project are listed below.

1. Literature review

Journals, articles or any materials regarding the project will be reviewed.

2. Inspection

The C_D and C_L will be determined and discuss with the supervisor between the relationship of angle of attack and vortex form at surface of the aerofoil.

3. Measurement

The measurement will be conducted at Turbo Machinery Lab. For aerofoil test will be conducted inside a wind tunnel. Measurement data of C_D and C_L will be collected and compare between two different cases.

4. Analysis and proposed solution

Analysis will be presented on how mathematical calculation to determine C_D , C_L and the angle of attack will help in creating vortex near the surface of the aerofoil as well as the optimum position/distance (x) of vortex generator to be determine to achieve the maximum velocity profile. Solutions will be proposed based on the analysis.

5. Report writing

A report on this study will be written at the end of the project.

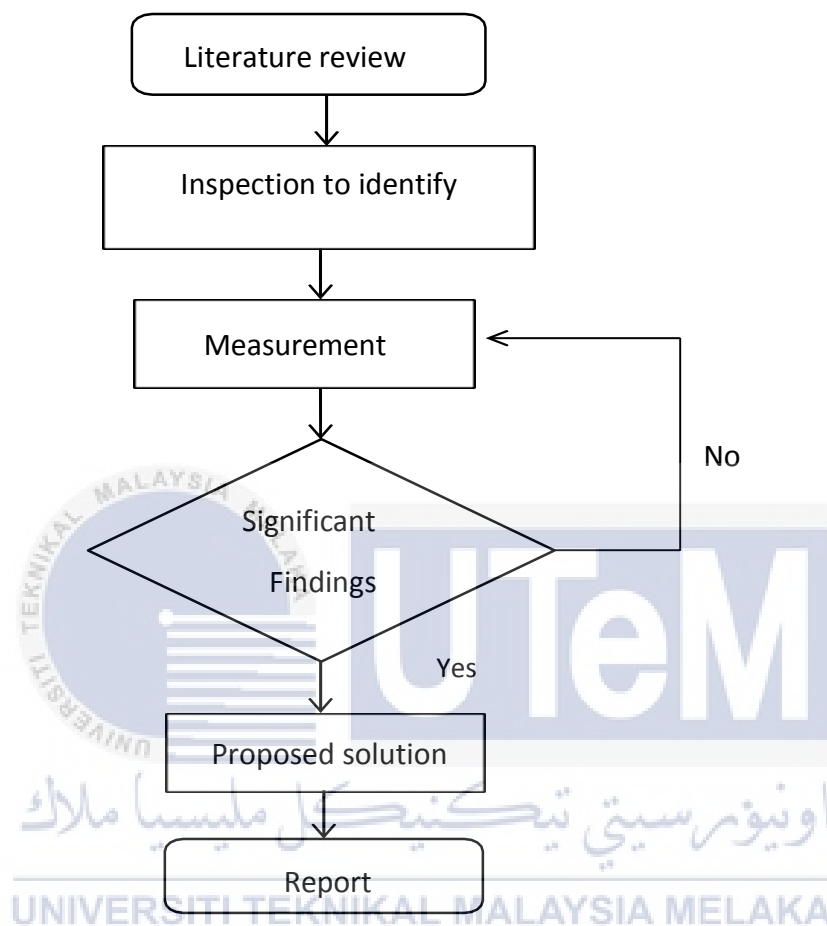


Figure 1.2: Flow chart of the methodology.

CHAPTER 2

LITERATURE REVIEW



2.1 Overview

اونيورسيتي تيكنيكل مليسيا ملاك
UNIVERSITI TEKNIKAL MALAYSIA MELAKA

For this chapter, a throughout investigation of the processes intricate with vortex generator is exhibited. It involves on describe and define the basic fundamental behind the procedures or processes required with the vortex produced. This will likewise involve experimental outcomes and findings of other researchers which will help with the design of a vortex generator. As a beginning, this chapter will start with the more common and essential feature of the vortex generator and gradually will concentrate on the proposed subject.

2.2 Background on Vortex Generator

A Vortex generators creates stream-wise vortex flow which fusion of multiple flow of boundary layer in wall-bounded flows. Vortex generator helps by increasing stream-wise velocity generates at the wall, average amount of momentum transfer towards it and mean. Consequently, the boundary-layer velocity profile at its higher form because of the great energy of fluid is pushed near to the wall and at its lowest form because it been pushed away. Overall, VGs conserve the flow to be steady by boundary-layer mixing processes, causing in delayed or even stopped boundary-layer separation. Accordingly, earlier discoveries from investigation relating active and passive VGs are presented.



2.2.1 Active Vortex Generator Jets



Despite the fact that the theory of active flow control was previously studied during middle of the twentieth century, it has merely turn into more common in the researchers' society during the past twenty five years. There is no geometrical structures required in an active VGJs which penetrate from the surface of an object into the mean flow. This has the advantage that VGJs do not contribute to parasitic drag in contrast to permanently deployed VVGs. Moreover, VGJs have the option to be activated when flow-separation control is needed, and to be deactivated when flow control is not needed. This feature creates this concept highly flexible and efficient.

(Johnston and Nishi, 1990) have investigated the configurations of tilted and pitched co- and counter-rotating circular VGJ arrays. Accordingly, it can be revealed for $\beta = 90^\circ$, that the produced stream-wise vortices remained similar to those from passive VVGs, that the mixing in the boundary layer was connected with the stream-wise vortices, and that the vortices effectively removed areas of separation. Those results correspond with the same vortex demonstrating analysis for the VVG and the VGJ simulations in this theory. Next, they also proved that the vortices from VGJs be likely to disperse faster compare to the passive VVGs.

Next, VGJ generates vortices through an injected jet with a velocity U_{VGJ} which pass in the boundary-layer flow through the actuator exit of diameter Φ_{VGJ} in a direction considered by the pitch and skew angles α and β , respectively which shown in Figure 2.01. Based on observation for this theory, the skew angle $\beta = 0^\circ$ is defined in the upstream direction. The jet injection is allowed using continuous or pulsating jet blowing. The greater total of potential setup parameter combinations will create an active VGJs. In the other hand, passive VVGs more likely to be more complex and require more times to demonstrate. This is one of the applied causes for the dominance of experimental research is difference with a smaller scope of study in computational studies.

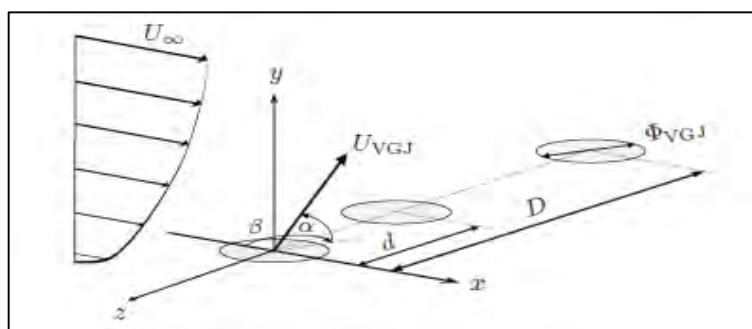


Figure 2.01: The VGJ actuator geometry and parameters, also showing the additional symmetry parameters d and D for pair and array configurations.

(<http://fluidsengineering.asmedigitalcollection.asme.org/article.aspx?articleid=1430651>)

2.2.2 Passive Vane Vortex Generators

During this past century, passive vane vortex generators (VVGs) are widely used for the purpose of controlling the flow separation. The word “passive” denoted as the VGs that create a stream-wise vortex without needing any extra external energy apply yet, the other advantage of using passive VVGs is the cause of greater overall drag. The solution for the great amount of drag can solve by installing a VVG which can be adjustable in any degree of angle for example the flap of aeroplane wings shown in Figure 2.02. The existence of parasitic drag is a transaction condition for the designer while it is not a simple task to make a prediction on drag penalties besides the difficulties of a stationary passive VVG arrangement a priori. Characteristically, VVGs are mounted normally on the surface of specimen, depending to the vane angle of incidence α towards the mean-flow direction. It is the most economical and fastest method to install the components for the purpose of passive VVGs in order to control the flow separation. Hence, it is commonly used in the aeronautic and automotive sector lately and scientist are keep on improving the performance based on fluid-mechanics and CFD studies.



Figure 2.02: Deployed flaps and spoilers uncover VGs close to the leading edge on a flap during landing. ([https://en.wikipedia.org/wiki/Spoiler_\(aeronautics\)\)](https://en.wikipedia.org/wiki/Spoiler_(aeronautics))))

Refer to (Pearcey, 1961), he is recommended which specific design standards for effective boundary layer flow control with VVGs. His research involved various designs of VVG which include co-rotating and counter-rotating VGs, multiple-row systems, and VVGs of dissimilar geometries. Figure 2.03 shows the counter-rotating setups and Figure 2.04(a) shows the characteristically cover VVG sets with fins mounted on a mirror-inverted method so that vortices with opposite-rotational directions are produced. This setup is the basic for the presentation of flow-separation control in two-dimensional flows when the span wise velocity section is zero also used as the guideline to conduct experiment in this research paper.

Next, for the comparison, Figure 2.04(b) shows the co-rotating setup, where VVG fins are mounted in the same method with respect to α consequently and generate vortices with the identical rotating directions. This setup is normally discover in three-dimensional flows such as in highly swept airplane wings across high current of cross-flows. Pearcey has performed an important research on passive VVGs for during past fifty decades and the parameters that were taking include is distance link adjacent VVG pairs (D), distance between tow VVG fins of a VVG pair (d), VVG chord (c^1) and last but not least the angle of incidence of the fin (α).

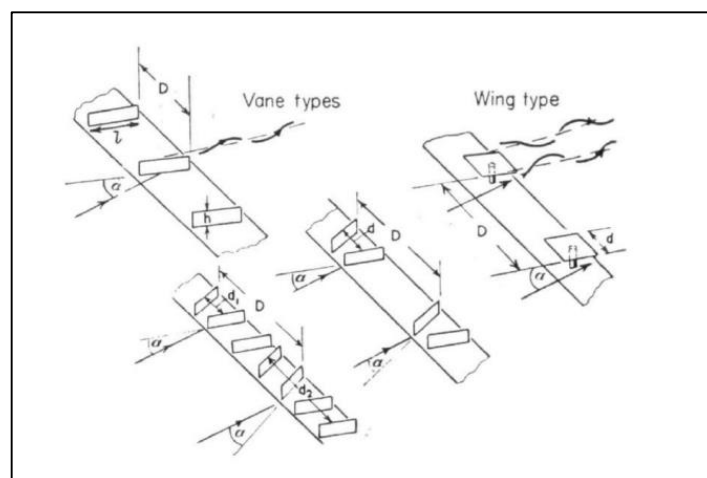


Figure 2.03: Types and notation of Pearcey's VVGs. Reference [Pearcey (1961)]

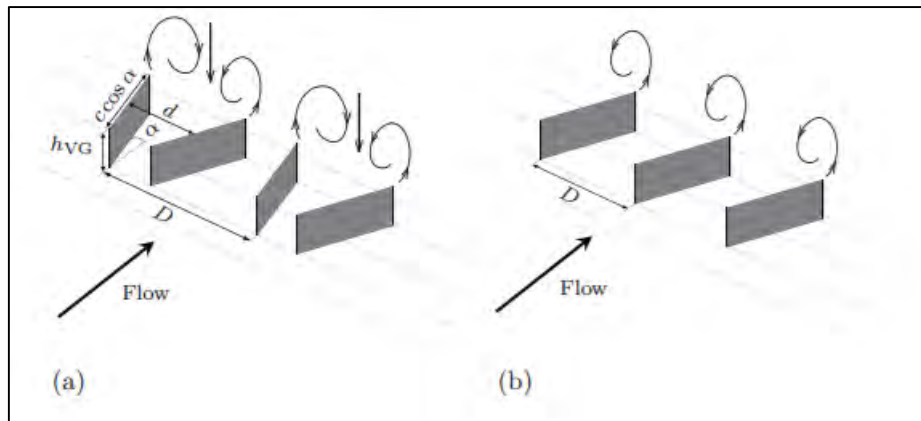


Figure 2.04: VVG setups and the notation: (a) counter-rotating common flow downward, and (b) co-rotating ($d = 0$) configurations. Reference [Pearcey (1961)]

2.2.3 Influence of Vortex Generator Vane/Fin Shapes

A study has been conducted by (Ho-Joon Shim, Ki-Jung Kwon, and Seung-O Park, 2017) state that the parameter of the shapes of VG's Vane/Fin make different in the result. The vortex generator with the height (h) is about boundary layer thickness is mentioned to as conventional vortex generator while the vortex generator with the of height (h) is smaller than local boundary layer thickness (δ) is mentioned to as low profile vortex generator or micro vortex generator. Some other data also shows that the low-profile vortex generator may correspondingly be efficient in spite of its smaller height for flow control as shown in Figure 2.05 and Figure 2.06.

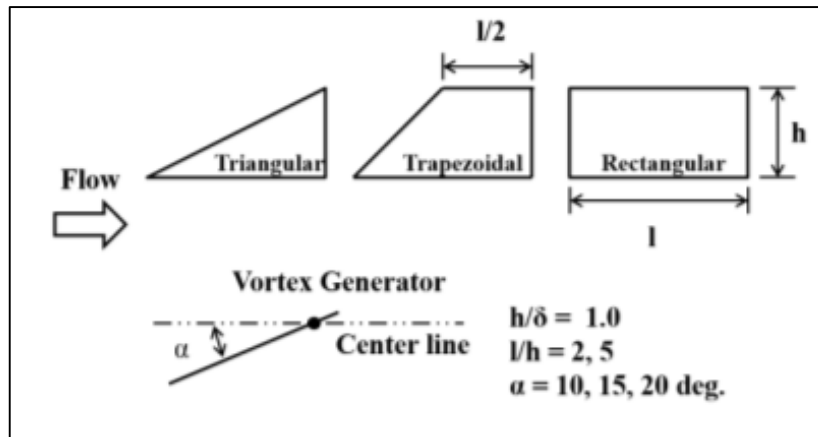


Figure 2.05: Geometries of Vortex Generators and Test Conditions. (Ho-Joon Shim, Ki-Jung Kwon, and Seung-O Park, 2017)

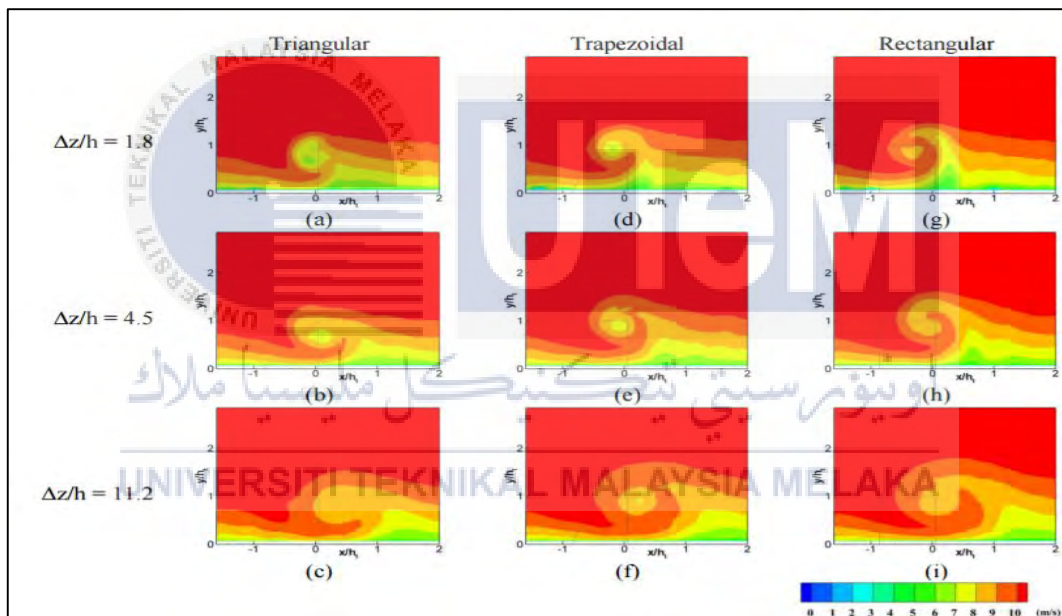
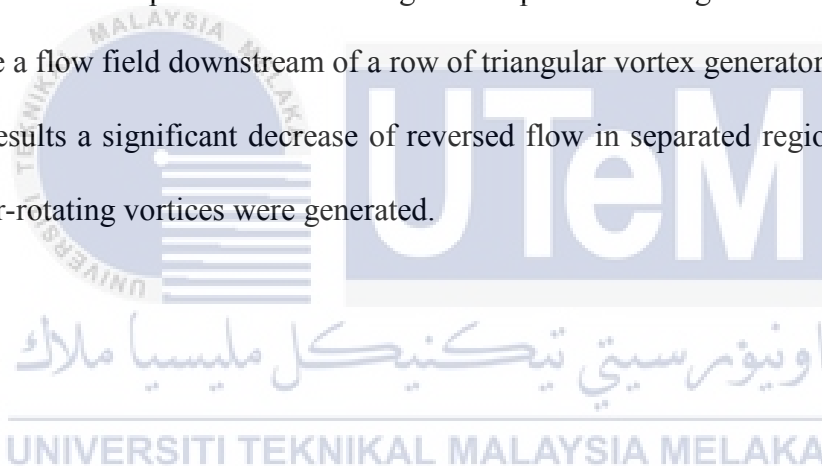


Figure 2.06: Mean streamwise velocity contours ($h/\delta = 1.0$, $l/h = 5$, and $\alpha = 10$ deg.) (Ho-Joon Shim, Ki-Jung Kwon, and Seung-O Park, 2017)

Based on previous study by (Ashill et al., 2001) he has conducted an experiment on wedge and triangular vane/fin types of vortex generators of $h/\delta = 0.3$ on a bump. Next, (Yao et al., 2002) measured flow field downstream of a single rectangular shape of vortex generator using stereoscopic particle image velocimetry (Stereo-PIV herein after). (Angele

and Muhammad-Klingmann, 2006) had conducted research on a divided boundary layer by using a rectangular vortex generator with three various heights and stream-wise positions. (Lin et al., 1991, 1994) did a research on wishbone and doublet vortex generator as well as method on how to evaluate boundary layer separation control using triangular and trapezoidal shapes of small surface installed vortex generators on a high lift aerofoil with a leading edge slat and a flap. (Godard and Stanislas, 2006) conducted a parametric research on angle of attack, length, transverse distance and etc. of vortex generators and verified both co-rotating and counter-rotating setup. All the research that had been conducted by them shows the result which the triangular shape of vortex generators generated high amount of drag improvement compared to the rectangular shape of vortex generators. (Velte et al., 2008) define a flow field downstream of a row of triangular vortex generators installed on a bump and results a significant decrease of reversed flow in separated region of the bump after counter-rotating vortices were generated.



2.3 NACA 0015 Aerofoil

NACA 0015 is a type of aerofoil. It has the maximum thickness of fifhteen percent at thirty percent of chord and has the maximum chamber of zero percent at zero percent of chord. According to (İzzet Şahin and Adem Acir, 2015), the lift and drag coefficient experimented inside a wind tunnel for NACA 0015 aerofoil model can be obtained with the maximum lift and drag coefficient were recorded as 0.75 and 0.15 at the angle of attack of sixteen degree. Next, lift and drag coefficient was mostly influenced by the angle of attack regarding mutually decreasing and increasing. If the condition where attack angle increased,

the lift and drag coefficient may also increase till a specific angle. After it reach till the specific angle, the lift coefficient will decreasing while the drag coefficient was increased. This condition was known as stall angle. The stall angle caused transition from laminar to turbulence flow throughout the aerofoil. This experiment also been conducted using CFD and Figure 2.07 show the results gain by using Spalart Allmaras, experimental and K-epsilon methods.

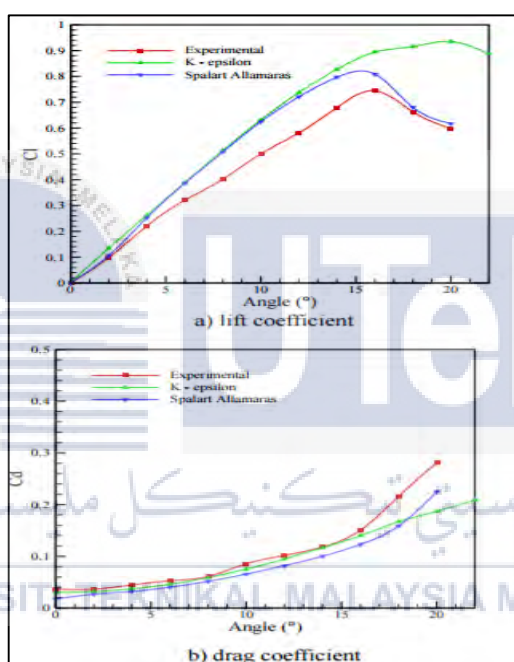


Figure 2.07: Experimental and Numerical Results. (İzzet Şahin and Adem Acir, 2015)

By using CFD, it can be seen that it is laminar flow throughout the NACA 0015 for the angle of attack between zero to fourteen degree. Then, the flow start to changeover turbulence as well as the pressure distribution at the attack angle of sixteen hence, the lift coefficient correspondingly decrease. Figure 2.08 shows the CFD simulation on NACA 0015.

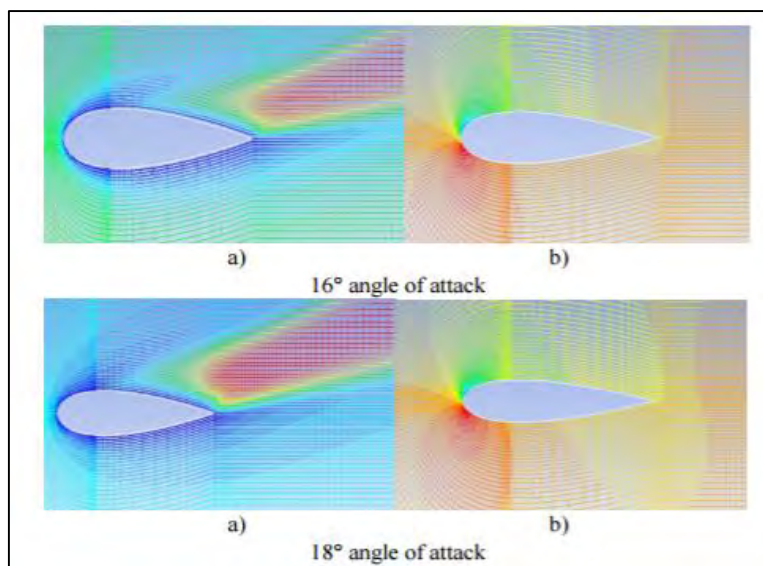
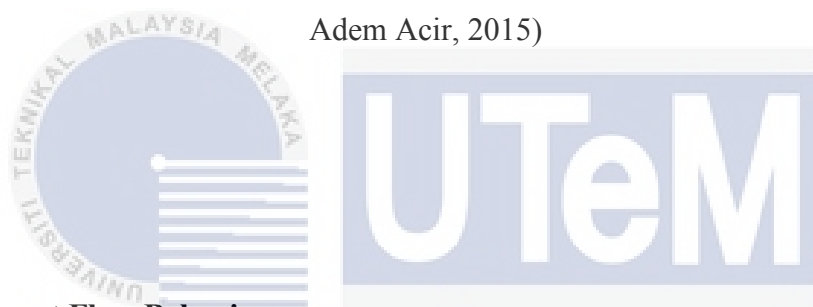


Figure 2.08: Distribution of Turbulence and b) Distribution of Pressure. (İzzet Şahin and

Adem Acir, 2015)



2.4 Different Flow Behaviour

اونيورسيتي تيكنيكل مليسيا ملاك

UNIVERSITI TEKNIKAL MALAYSIA MELAKA

2.4.1 Turbulent and Laminar Flow

By referring to (Aman Sharma, 2012), laminar flow is represented by layers or laminae of a moving air at the identical velocity and with the similar path. There is no exchanged in fluid between the laminae and there is no requirement for straight line flow for it. Basically, any types of fluid will flow accordingly with the surface contact and it is consider an ideal flow in laminar. Next is the description for turbulent flow. In a turbulent flow, the streamlines are unsystematically in pattern and it cause an exchange of fluid on the area of the surface contact. Besides that, turbulent flow will cause the different in

momentum. This is due to the transition of higher energy particles give it momentum to the lower energy particles. Almost all fluid flow shows the characteristic in some degree of turbulence.

Figure 2.09 below shows the separation of crest of convex surface of the laminar boundary layer on the top part of the figure and the bottom part shows the turbulent boundary layer stay attached longer with the point of separation taking place further downstream.



Figure 2.09: Turbulent and Laminar Boundary Flow. (Aman Sharma, 2012)

On top of that, Reynolds number is another important parameter of this aerofoil experiment. It influence the behaviour of fluid as well as boundary layer. Same parameter of Reynolds number will produce the same behaviour of flow. Equation below can be used to determine and calculate the amount of Reynolds number.

$$Re = v \times l \times 70000 \quad [0]$$

v----- (Flight speed)

l----- (Cord length in metre)

70000----- (Constant value of air (s/m²))

Reynolds number is depends on the distance, which normally refers to the cord length of a wing as well as the chord length of an aerofoil. Due to the chord length is various from the tip to root, the mean of an aerodynamic chord length is used to determine the wing's Reynolds number.

2.4.2 Delay in Flow Separation

(Kuethe, 1972) had mention where the amount of acoustic turbulences in the wake point can be reduced by using vortex generator over suppression of Kaeman vortex street formation. The used of vortex generator in automobile and aircraft sector bring benefits due to its low in cost and forceful unfortunately, there is a disadvantage that is not require which refer to drag which it against the fluid current flow stall cruise and cause flow separation. Generally, airplane are built-in with vortex generators during the stage of assembly, but it also likely to retrofit these generators to current designs.

Next, Figure 2.10 below shows the vortex generators which are in small rectangular or delta-shaped winglets, which have the function to delay separation and stall. These vortex generator components extend in the chord-wise direction and conservatively have a height which relates to the thickness of the boundary layers (Lin, 2002). Other research has been revealed that devices with the height about ten percent of the boundary layer thickness are legitimately effective and have fairly low drag (Lin, 2002; Godard and Stanislas, 2006). Vortex generators bulge out into the boundary layer and have incoherence that generate either co-rotating or counter-rotating stream-wise vortices, dependent on device angle. The produced vortices develop momentum exchange in the boundary layer which providing an

actual mixing region of over three times the height of the device (Lin, Selby and Howard, 1991).

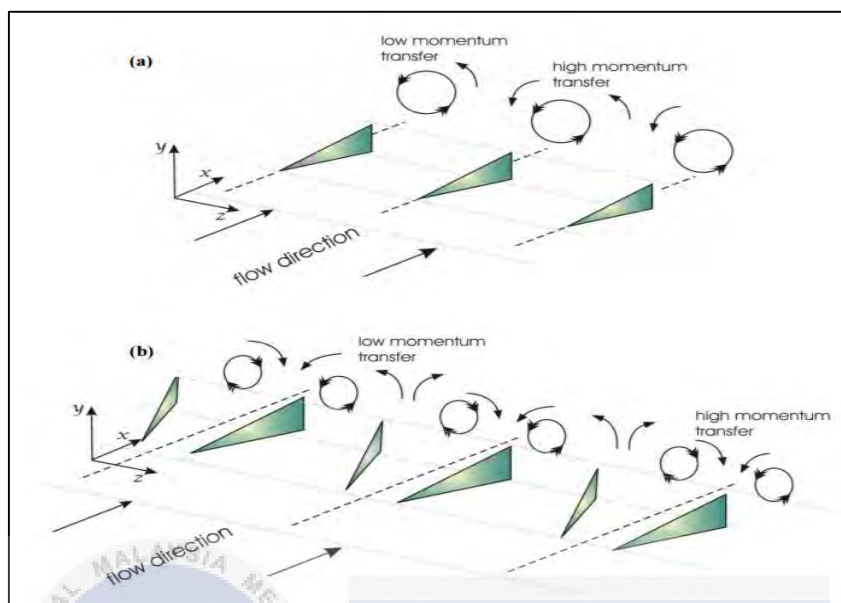


Figure 2.10: (a) Co-rotating Vortex Generator Configuration (b) Counter-rotating Vortex Generators Configurations [Reference: (Godard and Stanislas, 2006)].

Besides that, the disadvantage related with leading edge delays is that the development of vortex bursting can take place, which it can cause a structural defect of the airplane tail fragment (Lee, Brown, Zgela and Poirel, 1990) and attack rock due to the high degree of stream instability. This vortex helps in preserving flow attachment on top of the surface of the airplane wing component (Thompson, 1997), letting the wing to generate lift over the estimated stall angle. Leading delays or strakes have slight influence on the performance of the airplane at cruising situations but at uncertain to high angles of attack every leading edge delay begins to produce a high-swirl vortex shown by Figure 2.11.

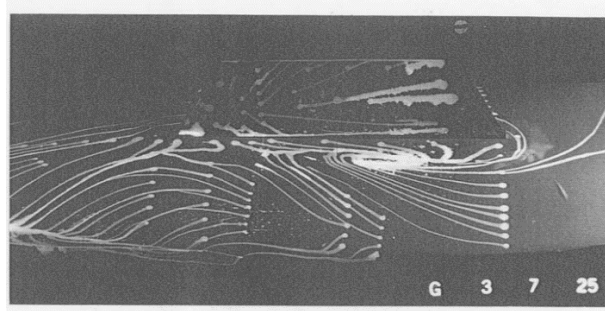


Figure 2.11: Visual of Swirl Vortex Pattern on the Leading Edge Upper Surface

[Reference: (Thompson, 1997)].

Moreover, other technique used to generate counter-rotating streamwise vortices on the pressure surface of an aerofoil is by installing tiny serrations along the pressure surface slightly on the front of the stagnation point (Soderman, 1972), as shown in Figure 2.12. Related performance enhancements involved improved maximum lift coefficient with small drag effects at low angles of attack and reduced drag force at high angles of attack (Soder, 1972). Although the serrations are installed on the pressure surface of the aerofoil, they essentially result the flow over the pressure surface from the time when the stagnation point is recognised to move at the pressure surface location with increasing angle of attack. Furthermore, the size, position and spacing are known as the important parameters. It was as well initiate that the tiniest serrations located as close as possible in front of the stagnation point contributed to the major improvements in performance.

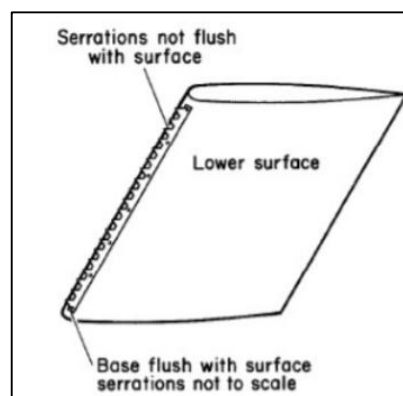


Figure 2.12: Leading edge serrations [Reference : (Soderman, 1972)]

2.4.3 Stall Cells

Stall Cells act on the suction sideways of wings with the angles of attack about maximum lift. They have existed reported on wing prototype with several types of tip cure which referred to wall to wall models with or without wall suction (Gregory et al, 1955; Wokoeck et al, 2006), tip with end plates (Yon and Katz, 1998), free tip (Winkelmann and Barlow, 1980), and can form on both low and high aspect ratio (AR) wings (from AR = 1.5 in Velte and Hansen (2012) to AR = 12 in Schewe (2001)). They have been testified to move in the span wise path (Yon and Katz, 1998; Zarutskaya and Arieli, 2005) or even form and vanish in an apparently random way (Gregory e tal., 1971, Gregory and O'Reil, 1970). It is majorly approved that for adequately high Re number ($Re > 0.3 \times 10^6$) and turbulence intensity (T.I. > 0.1%) SCs are dynamic structures.

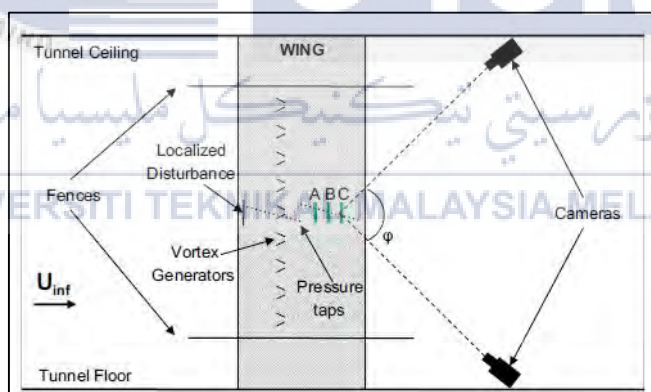


Figure 2.13: Plan in schematic view of the test set-up displaying the wing, the barriers, the pressure taps at the centre of the wing span, the stabilising disturbance and the Stereo PIV cameras along with the measurement planes at $x/c = 0.6$ (plane A), $x/c = 0.7$ (plane B) and $x/c = 0.8$ (plane C). The camera contained angle (ϕ) for plane C is also indicated.

[Reference :(Marinos Manolesos and Spyros G.Voutsinas, 2015)]

According to (Manolesos and Voutsinas, 2013), the naturally unsteady SCs can be become stable by means of a huge sufficient spanwise disturbance. In addition, a zigzag (ZZ) tape was mounted on the wing suction surface with its centre for 10% from its span, which performed as a stabilising device. The ZZ tape efficiently enforced the fluid current to form a stable SC. To be clarified, the ZZ tape is not to be used as the generating device for the SCs, which generate on the wing suction surface with or without the localised disturbance.

During the previous study, the similar balance mechanism and the identical wing model surveyed in ((Manolesos and Voutsinas, 2014); (Manolesos et al., 2013), (Manolesos and Voutsinas, 2013)) were used. The fluid current using the ZZ tape has the equal total of separated flow for angles of attack $\alpha > 9^\circ$ and for Re numbers reaching from 0.5×10^6 till 1.5×10^6 . It was clarified that the ZZ tape successfully forces the fluid current to determine one of the potential modes.

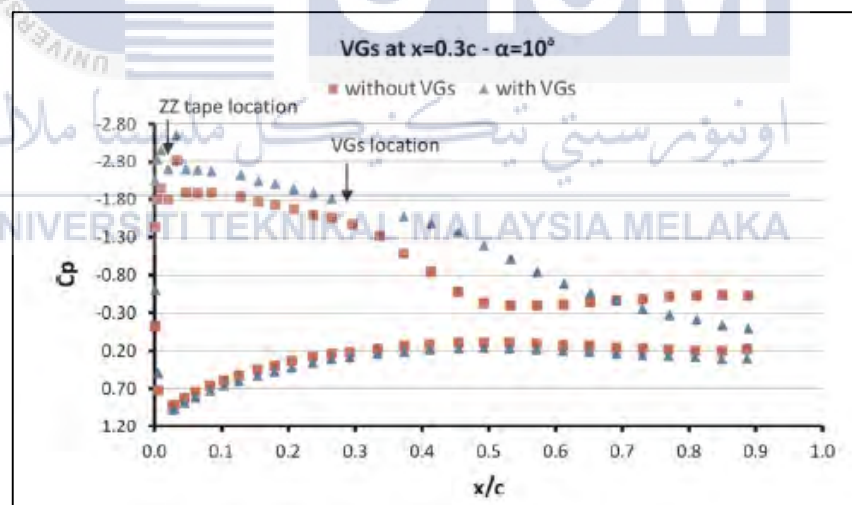


Figure 2.14: Pressure distribution along the wind chord for a wing with and without VGs at $\alpha = 10^\circ$. [Reference : (Marinos Manolesos and Spyros G.Voutsinas, 2015)]

(Moss and Murdin, 1971) is the only researcher that obtained reliable result regarding SC control with the main and only accepted positive attempt to delay SC formation using VGs was conducted on a NACA 0012 aerofoil, with the Re numbers of 0.9×10^6 and 1.7×10^6 . Forty years later, (Velte and Hansen, 2012) testified the onset of SCs at post-stall angles of attack on a DU 91-W2-250 profile with VGs with the same Re number of 0.9×10^6 .

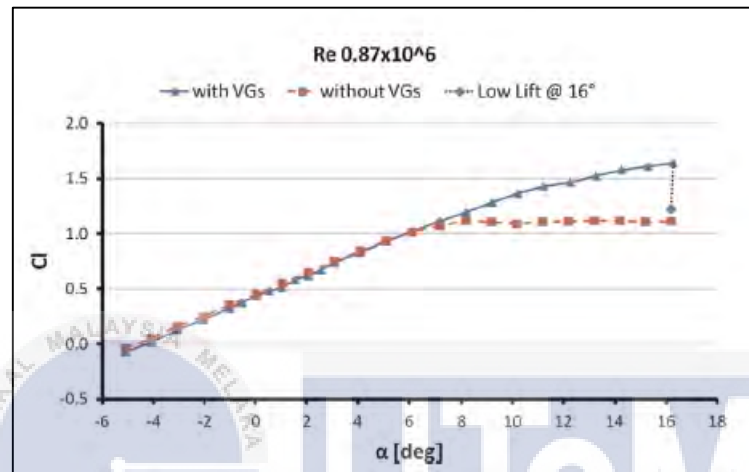


Figure 2.15: Experimental lift coefficient polar for a wing with and without VGs.

[Reference : (Marinos Manolesos and Spyros G.Voutsinas, 2015)]

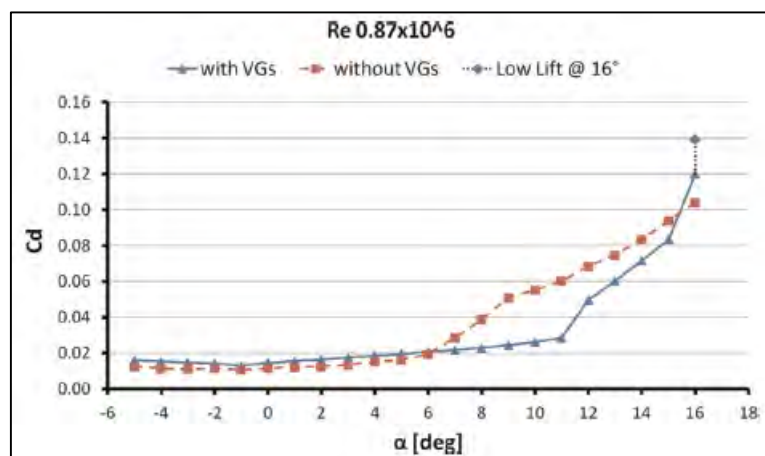


Figure 2.16: Experimental drag coefficient polar for a wing with and without VGs.

[Reference : (Marinos Manolesos and Spyros G.Voutsinas, 2015)]

2.4.4 Separation and Reverse Flow

Separation denotes as the detachment of the boundary layer from the airfoil. The description for a two-dimensional situation is as follows. With increasing angle of attack the circulation increases and the suction peak near the leading edge becomes deeper. This means that the velocity just outside the boundary layer near the suction peak becomes very high. The suction peak is located near the stagnation point where the boundary layer is still very thin (Figure 2.17). Thus the velocity gradient in the boundary layer, and thereby the viscous shear stress, becomes very high. This viscous shear converts kinetic energy from the boundary layer flow into heat (Corten, 2001).

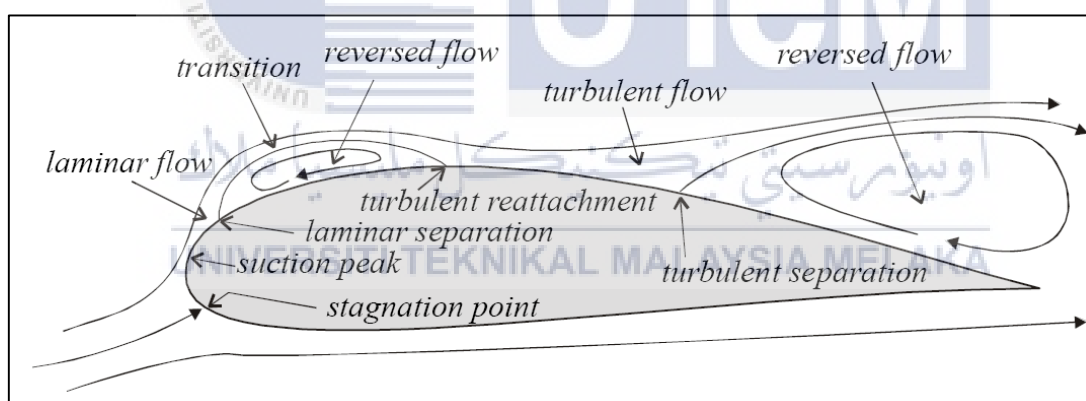


Figure 2.17: Qualitative Representation of Separation Types (Corten, 2001)

When the flow has passed the suction peak, four quantities or effects will determine whether it will reach the trailing edge. First, the remained speed (kinetic energy); second the trajectory of the viscous shear over the surface; third the trajectory of the adverse pressure gradient which decelerates the flow and fourth the momentum that will be transferred from

the main stream via viscous and turbulent stress in the boundary layer. The integral of the shear stress from the stagnation point to a certain position further downstream determines the kinetic energy losses. With increasing angle of attack, the suction peak becomes deeper since the curvature of the flow around the leading edge increases. The deeper this suction the more kinetic energy is lost by shear, and at a certain angle the flow does not reach the trailing edge any more. At a certain position it comes to a standstill and this position is called the separation line. Downstream from the separation line the pressure gradient accelerates the air towards the suction peak and this causes reversed flow. For two-dimensional flow, there are two types of separation; leading edge separation and trailing edge separation.

Leading edge separation can appear as a long bubble and a short bubble. The long bubble type of leading edge separation is a laminar separation type and gives a gradual decrease of the lift curve slope. The bubble grows with increasing angle of attack towards the trailing edge. It occurs on thin airfoil sections in combination with low Reynolds numbers in the order below 5×10^5 . For the short bubble type, above a certain angle of attack such bubbles suddenly burst and cause a sudden lift drop and drag increase. This occurs on thin airfoil sections with a round nose and low camber.

The trailing edge type of separation is a gradual type of separation, which starts at the trailing edge and moves forward with increasing angle of attack. This occurs on thick or cambered airfoils with a round nose, which have a less deep suction peak, so the trailing edge becomes the preferential location for the onset of separation.

2.5 Forces Exerted Towards Aerofoil

According to Newton's second law of motion, lift and drag force of a body is directly influence by the changing of momentum of fluid with period. An aerodynamicist's body normally define the relation between the effect of mass on lift and drag to the air density. The governing equation for this case is given an assumption on momentum effects on lift force. Hence, lift and drag force is depend on the square of the velocity.

2.5.1 Pressure Distribution

In the study of aerofoil by (Dr. J. M. Meyers, Dr. D. G. Fletcher and Dr. Y. Dubief, 2013), method used to estimate the aerodynamic forces is by measuring the surface pressure distribution and integrate that over the aerofoil surface area. Pressure distribution is acts normally toward the surface, hence the curvature must be recognised at the area of investigation. On top of that, the relative angle facing the wind's direction made an effects towards pressure distribution. The summation of forces regarding pressure distribution that exerts on the wing is:

$$\vec{F} = \oint -(P \cdot \vec{n}) dA \quad [1]$$

Variable that is been take into account is the flow of wind in x-direction. Hence, the resultant force can be neglect and define horizontal and vertical components to improve the aerodynamic drag and lift force:

$$D = F_x = \int -P(\sin(\alpha + \phi)) dA \quad [2]$$

$$L = F_y = \int -P(\cos(\alpha + \phi))dA \quad [3]$$

Due to various condition of wind, non-dimensional representations are required based on the pressure coefficient:

$$C_{P_x} = \frac{P_x - P_\infty}{\frac{1}{2}\rho_{air}U_\infty^2} = \frac{P_x - P_\infty}{q_\infty} \quad [4]$$

$$q_\infty = \frac{1}{2}\rho_{air}U_\infty^2 \quad [5]$$

C_p indicate the change between local static pressure and free-stream (at ∞) static pressure, non-dimensional by the free-stream dynamic pressure. Figure 2.18 shows the coefficient distribution between C_p against x/c .

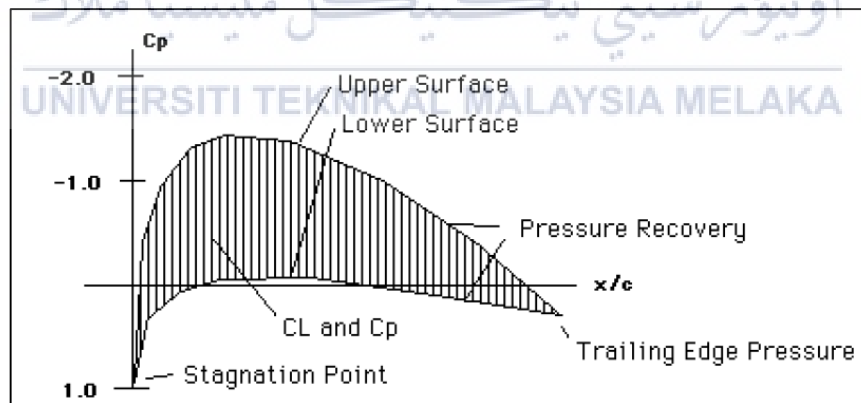
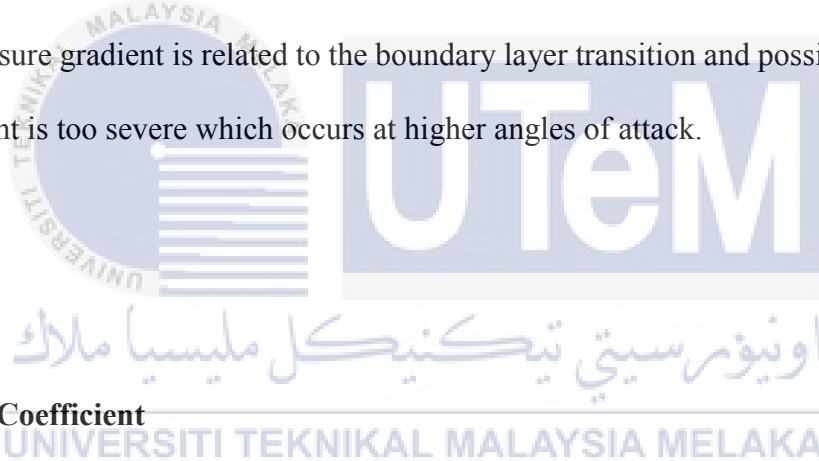


Figure 2.18: Coefficient Pressure Distribution over an Aerofoil (Dr. J. M. Meyers, Dr. D.

G. Fletcher and Dr. Y. Dubief)

The value of C_p at the aerofoil stagnation point is unity. This relate with the Bernoulli relation and description on the stagnation point ($U_{stag} = 0$). It then declines fast on both of the upper and lower surfaces and finally improves to a small positive value of C_p near the trailing edge. The upper surface pressure is lower (plotted higher on the usual scale) compare to the lower surface C_p for this case of study but it is unnecessary. The lower surface occasionally transmits a positive pressure, however at several design states is actually dragging the wing downward. The pressure at the trailing edge is dependent to the aerofoil parameter and shape nearby the trailing edge. High positive values of C_p near the trailing edge indicate additional severe adverse pressure gradients. Next, for the pressure recovery region, the pressure rises from its smallest number to the number at the trailing edge. This adverse pressure gradient is related to the boundary layer transition and possibly separation, if the gradient is too severe which occurs at higher angles of attack.



2.5.2 Lift Coefficient

According to (John D. Anderson, 1991), lift force be able to calculate if the distribution of dynamic pressure and shear force on the full body are identified. Consequently, the lift coefficient (C_L) can indicate with the formula shown below:

$$C_L = \frac{L}{\frac{1}{2} \rho v_e^2 A}$$

[6]

L-----Lift Force

ρ ----- Density of air

v----- Upstream wind velocity

A-----Frontal area

The value of lift force can be obtain by rearranging the lift coefficient equation:

$$L = \frac{1}{2}\rho v^2 C_L A \quad [7]$$

2.5.3 Drag Coefficient

Regarding to (John D.Anderson, 2007), total drag is formed by both pressure and shear forces. Equation below is refer to the drag coefficient:

$$C_D = \frac{D}{\frac{1}{2}\rho v_\infty^2 A} \quad [8]$$

D-----Drag Force

ρ ----- Density of air

v----- Upstream wind velocity

A-----Frontal area

The value of lift force can be obtain by rearranging the lift coefficient equation.

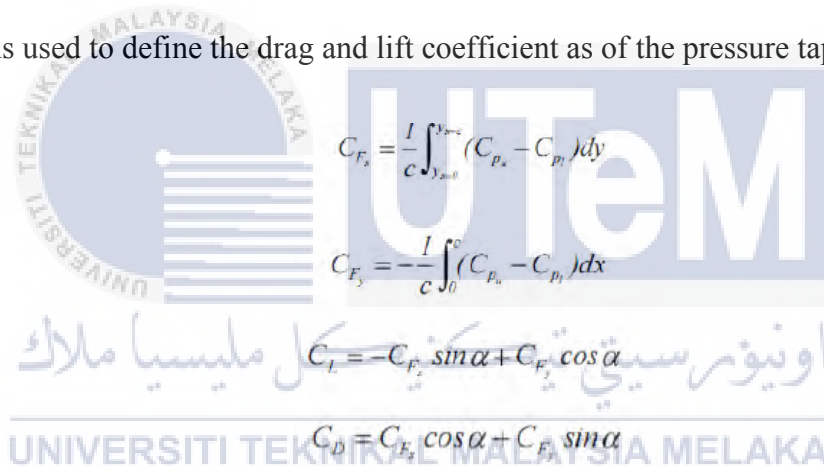
$$D = \frac{1}{2}\rho v^2 C_D A \quad [9]$$

2.6 Analysis

For NACA 0015, the trapezoidal principle is used as the numerical method required the integration of the statistics measurement. Equation below shows the trapezoidal method. (Steven D. Miller, 2008)

$$I(f) \approx \frac{[f(a) + f(b)]}{2} (b - a)$$

It is a modest symmetrical calculation toward area under the curve of function f by acquiring the modification between whichever two points of (a) and (b) is linear. Next shows the equations used to define the drag and lift coefficient as of the pressure tap records.



$$C_{F_x} = \frac{1}{c} \int_{y_{x=0}}^{y_{x=c}} (C_{p_u} - C_{p_l}) dy$$

$$C_{F_y} = -\frac{1}{c} \int_0^c (C_{p_u} - C_{p_l}) dx$$

$$C_L = -C_{F_x} \sin \alpha + C_{F_y} \cos \alpha$$

$$C_D = C_{F_x} \cos \alpha + C_{F_y} \sin \alpha$$

Entirely by using the trapezoidal rule showed, integration of the equation can be achieved. The moment coefficient is calculated around the area of chord situation assuming the anti-clockwise direction as the positive vector. These is completed by using the next calculation of the moment coefficient.

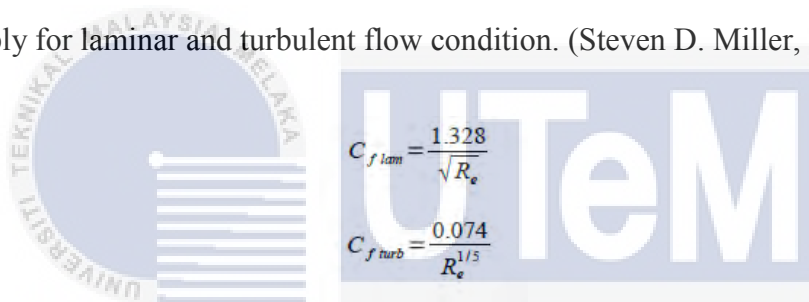
$$C_{M_{x_0}} = -\frac{1}{c^2} \int_{y_{x=0}}^{y_{x=c}} y(C_{p_u} - C_{p_l}) dy - \frac{1}{c^2} \int_0^c (C_{p_u} - C_{p_l})(x - x_0) dx$$

Furthermore, NACA 0015 aerofoil model is moderately low thickness and symmetric in parameter hence, low thickness of aerofoil concept is use appropriately in

determining the theoretical values of the moment, drag and lift forces. The following equation relates the coefficient of lift to the angle of attack for thin symmetrical aerofoils.

$$C_L = 2 \pi \alpha$$

Moreover regarding the concept, the coefficient of the moment near the middle aerodynamic of a low thickness symmetrical aerofoil is assume as zero as the middle of aerodynamic is positioned at the chord area or else $x/c = 0.25$. Thus, the coefficient of moment at every angle of attack at the chord area is assume zero according to concept. Next, the theoretical drag force of NACA 0015 aerofoil can be determined by creating a flat plate theory and considering the laminar and turbulent conditions individually. Below shows the equation apply for laminar and turbulent flow condition. (Steven D. Miller, 2008)



$$C_{f \text{ lam}} = \frac{1.328}{\sqrt{R_e}}$$

$$C_{f \text{ turb}} = \frac{0.074}{R_e^{1/5}}$$

With the intention of determine the total drag coefficient, the frictional coefficients are included later on to determine the drag coefficient. The best method to record the drag force is by pass through the wake downstream of NACA 0015. It is considered complete by investigating the momentum reduce of the fluid caused by the viscous forces by relating the momentum formula to a fix measurements all over the aerofoil.

As shown below is the equation of the drag force and normalized with the dynamic pressure. The symbol of S_2 in the equation refers to the surface area of the downstream aspect of the fix volume while u_2 refer to the velocity pass through it.

$$D = \rho b \int_{S_2} u_2 (U_{inf} - u_2) dS$$

2.7 Discussion

- a) Vortex Generators conserve the flow to be steady by boundary-layer mixing processes, causing in delayed or even stopped boundary-layer separation. There are various electrode configurations.
- b) The vortex generator with the height (h) is about boundary layer thickness is mentioned to as conventional vortex generator while the vortex generator with the of height (h) is smaller than local boundary layer thickness (δ) is mentioned to as low profile vortex generator or micro vortex generator.
- c) Lift and drag coefficient was mostly influenced by the angle of attack regarding mutually decreasing and increasing. If the condition where attack angle increased, the lift and drag coefficient may also increase till a specific angle. After it reach till the specific angle, the lift coefficient will decreasing while the drag coefficient was increased. This condition was known as stall angle. The stall angle caused transition from laminar to turbulence flow throughout the aerofoil.
- d) Reynolds number influence the behaviour of fluid as well as boundary layer. Same parameter of Reynolds number will produce the same behaviour of flow.
- e) Pressure distribution is acts normally toward the surface, hence the curvature must be recognised at the area of investigation.
- f) Devices with the height about ten percent of the boundary layer thickness are legitimately effective and have fairly low drag.
- g) For NACA 0015, the trapezoidal principle is used as the numerical method required the integration of the statistics measurement.
- h) The suction peak is located near the stagnation point where the boundary layer is still very thin

CHAPTER 3

METHODOLOGY



3.1 Introduction

Vortex generator are varies in designs and geometries. The main purpose of this research is to determine the C_L and C_D produce towards the NACA 0015 aerofoil with the surface area of 13 cm x 13 cm. Comparison between baseline case and modify case (applying vortex generator) been made. The methodology applied in this study is based on experimental study on the effect of vortex generator to aerodynamics performance of aerofoil by using aerofoil model NACA 0015 and two different shapes of vortex generator at the leading and trailing edge. The air velocity is set at 13 m/s as the fix variable. To conduct the experiment, there are variables that need to be consider such as:

- i. Configuration of SDBD
 - Parameter of aerofoil (NACA 0015).
- ii. Positioning of vortex generator
 - Leading and trailing edge.
- iii. Angle of incidence
 - Angle of attack is set to be 0 °, 5 °, 10 °, 15 ° and 20 °.



3.2 Flow Chart

Below shows the flow chart (Figure 3.1) of methodology procedure of the whole experiment in briefly step by step.

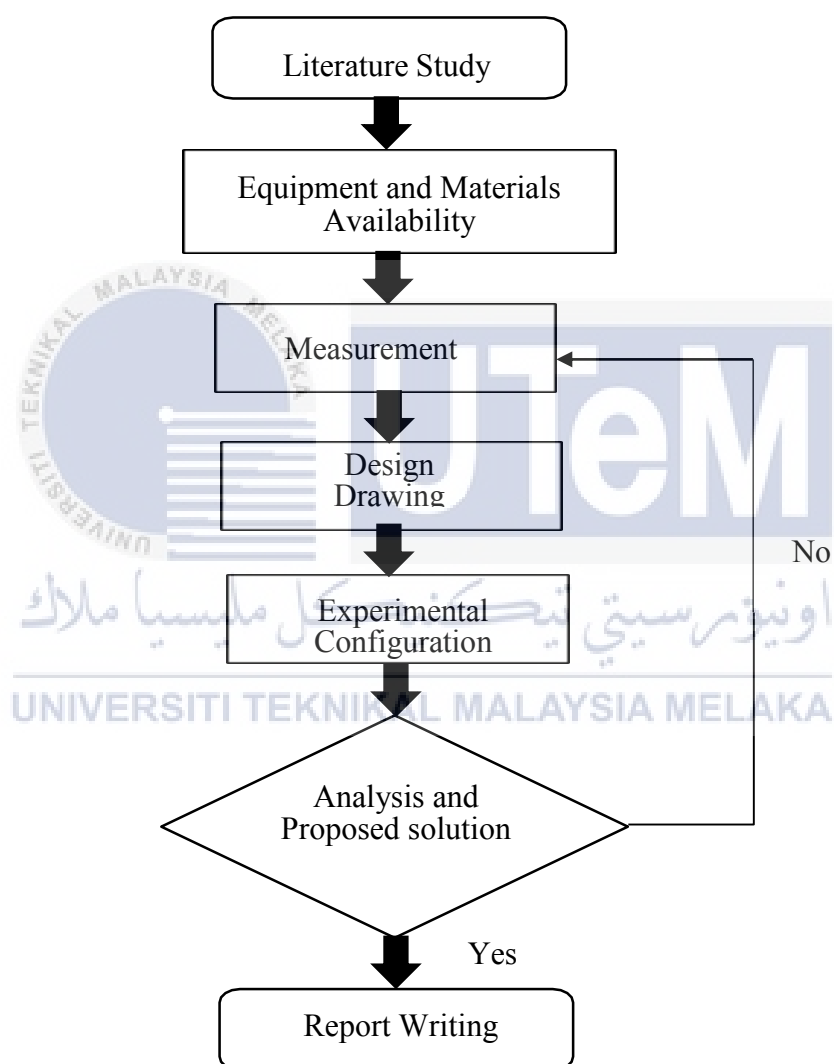


Figure 3.1: Flow Chart of the Methodology

3.3 Experimental Equipment

3.3.1 MP 130D Subsonic Wind Tunnel, Downstream Fan

To conduct this experiment, a fix amount of 13 m/s wind velocity is require. Hence, one of the best wind tunnel that can be use is MP 130D Subsonic Wind Tunnel, Down Stream Fan as shown in Figure 3.2 – Figure 3.5. The wind tunnel is a vertical axis wind tunnel model or also known as VAWT. This MP 130D model equip with seven blade fan which is a aerofoil design cast aluminium to ensure maximum aerodynamic efficiency, minimum turbulence and the speed are adjustable by using an inverter.

Next, four alike spaced static pressure taps are attached to a manifold at contraction section to reduce the special effects from a model and air velocity is shown by an inclined manometer. A graph of manometer reading using air velocity is provided. Models are fixed on two components load cell support with displays for measurement of drag and lift. Model holder can be rotated to let quick change on the angle of incidence. This angle is indicated on an angular scale at the base of the holder.

The tunnel is fixed on a self-contained bench with castors. The technical data is shown below:

- *Fan : 480 mm. diameter
- *Motor : 3.7 kW, 220V/280V, 3 Ph., 50 Hz.
- *Inverter : 5 KVA
- *Contraction area ratio: 7:1

*Test section : 300 mm. x 300 mm. x 450 mm. long

*Maximum air velocity: Over 30 m/s.

*Power supply : 220 V, 1Ph., and 50 Hz.



Figure 3.2: Front View of MP 130D Subsonic Wind Tunnel.



Figure 3.3: The motor for MP 130D Subsonic Wind Tunnel.



Figure 3.4: Speed Control Module and Indicator Module.



Figure 3.5: Wind Velocity, Test Section.

3.3.2 NACA 0015 Aerofoil

NACA 0015 aerofoil model with the surface area of 13 cm x 13 cm is used. It being placed vertically inside the wind tunnel chamber with incidence angle of 0, 5, 10, 15, 17, 18, 19, and 20 degree.

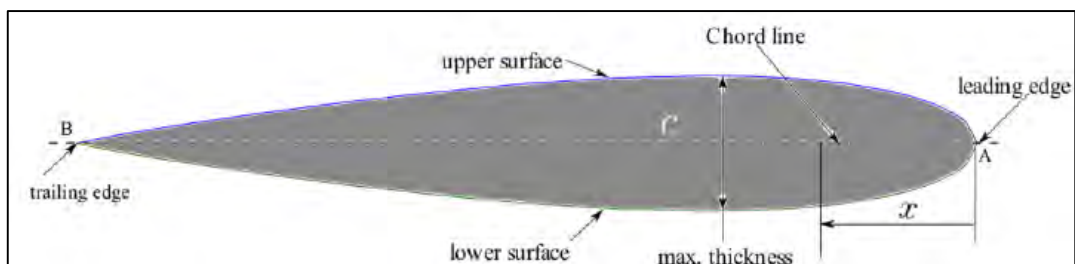


Figure 3.6: NACA 0015 with labels.

(https://www.researchgate.net/figure/267210609_fig1_Figure-1-NACA-0015)

3.3.3 Vortex Generator

Vortex generator with the length of 15 mm and 3 mm in thickness is used during this experiment. It come with two different vane shape which are the rectangular shape and fin shape. Both are create using 3D printing machine. The vortex generators is mounted with the angles of 60 and 120 degree and 2 cm from the leading end and 2 cm away from the trailing edge.



Figure 3.7: Fin and Rectangular Shaped of Vortex Generator.

3.3.4 CubePro Duo 3D Printing Machine Model

A model of CubePro Duo 3D printing machine (Figure 3.8) is used to print out the NACA 0015 and vortex generator designs. The sketch of NACA 0015 and vortex generator design by using SolidWorks software must be convert into STL format to become compatible with CubePro Duo software. By using CubePro Duo's software, any editing procedures can be done during the 3D printing process. The printing process take about thirty minutes for vortex generators and five hours for NACA 0015 aerofoil.

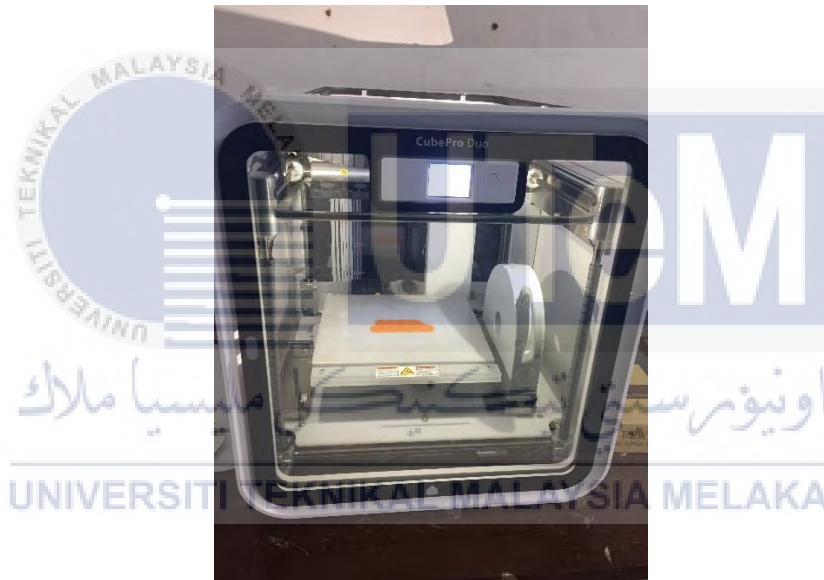


Figure 3.8: CubePro Duo 3D Printing Machine Model.

3.3.5 Acrylonitrile butadiene styrene (ABS)

ABS is used as the 3D printing materials due to its durability compare to other materials of 3D printing such as PLA (PolyLactic Acid) and PVA (Polyvinyl Alcohol). The ABS that been used has the 1.76 mm in diameter and come with several in colours.



3.4 Design

3.4.1 Material Description and Design Drawings

Next are the design drawings of the NACA 0015 with mounted vortex generator. Fabrication process is needed to assemble all the components together. The required

components to run the experiment are NACA 0015, rectangular shaped vortex generators, fin shaped vortex generators and side plats. For NACA 0015 and vortex generators, the material used for the 3D printing process is ABS filament while for the side plat, acrylic plat with thickness of 3 mm is used. These components is mount on the aerofoil by using double sided tape during the experiment setup.

3.4.1.1 NACA 0015



Figure 3.10: NACA 0015, Surface Area = 13 cm x 13 cm

Figure 3.10 shows the design of NACA 0015. For this thesis, aerofoil type NACA 0015 is used. It has the surface area of 13 cm x 13 cm and has the maximum thickness of 15 % at 30 % of chord and has the maximum chamber of 0 % at 0 % of cord. The design take about five hours to produce using CubePro Duo 3D printing machine and using ABS filament.

3.4.1.2 Side Plat

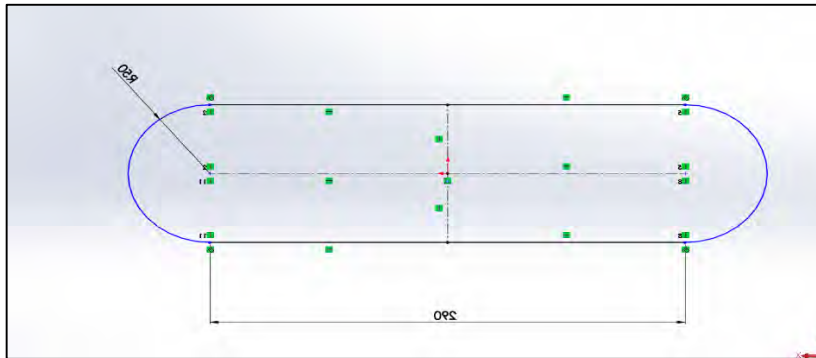


Figure 3.11: 2D Sketch of Side Plat.

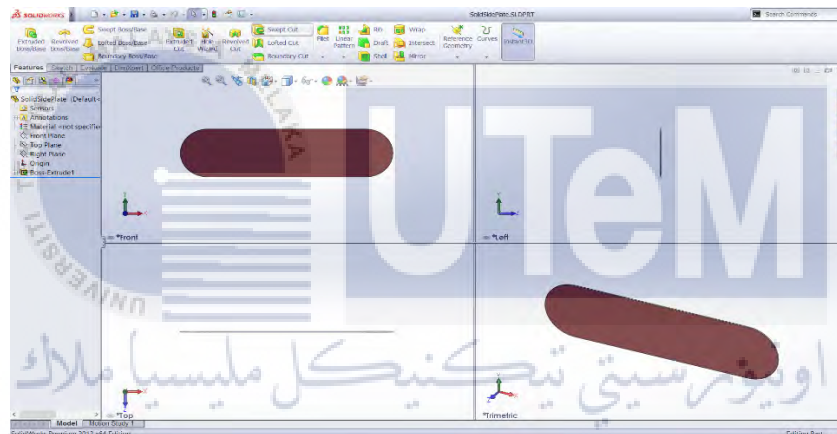


Figure 3.12: 3D Views of the Side Plats.

Side plat is used to prevent any flow separation at the side of the aerofoil. The purpose of this experiment is only focus on the surface of the aerofoil. The side plat has the length of 29 cm and half circle on sides with diameter of 5 cm. Acrylic plat is used to fabricate this component.

3.4.1.3 Vortex Generators

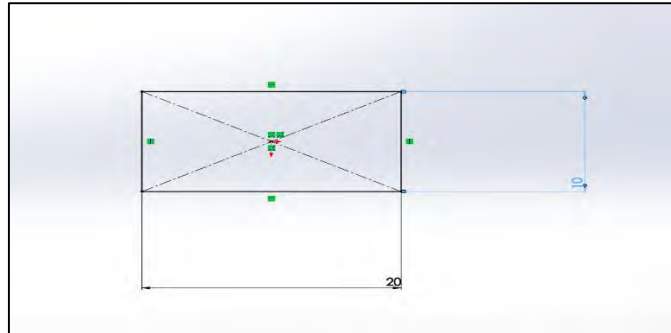


Figure 3.13: 2D Sketch for the Rectangular Shaped Vortex Generator

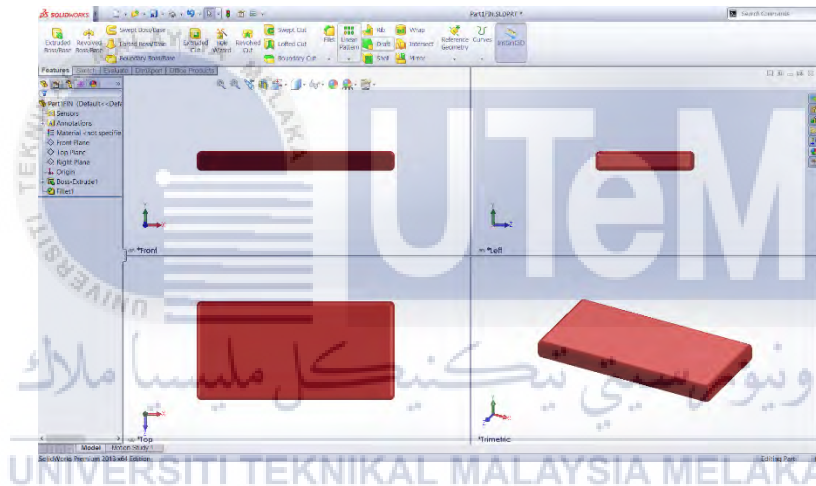


Figure 3.14: 3D Sketch Views of the Rectangular Shaped Vortex Generator

Figure 3.13 and 3.14 shows the design of the rectangular shape vortex generator. It has the dimension of 2 cm length x 1 cm height x 0.3 cm thickness.

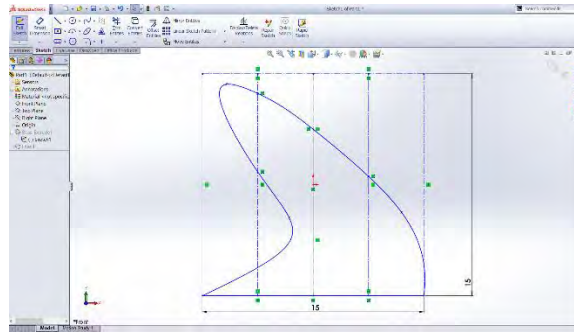


Figure 3.15: 2D Sketch for the Fin Shaped Vortex Generator

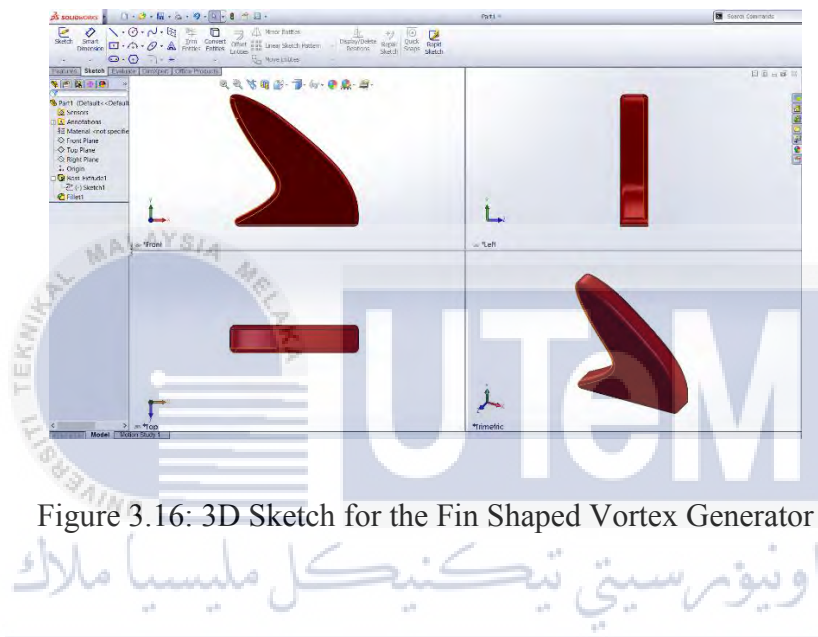


Figure 3.16: 3D Sketch for the Fin Shaped Vortex Generator

Figure 3.15 and 3.16 shows the design of the fin shape vortex generator. It has the dimension of 1.5 cm length x 1.5 cm height x 0.3 cm thickness.

Both type of vortex generators is using ABS filament material during 3D printing process and it takes thirty minutes to produce. Each design required four identical models to be produced and being placed at the trailing and leading edges of the aerofoil (NACA 0015). For this experiment, vortex generators are used to delay separation and stall with counter rotating condition.

3.4.1.4 Model Assemble

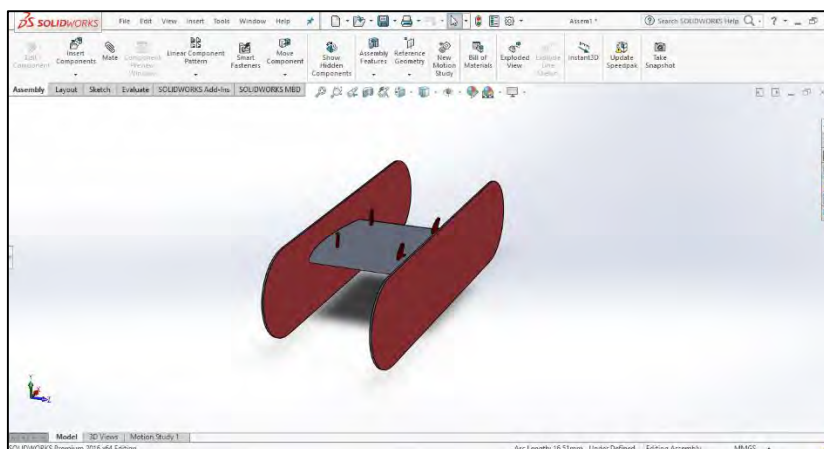


Figure 3.17: Assembly of Vortex Generator Experiment (Fin)

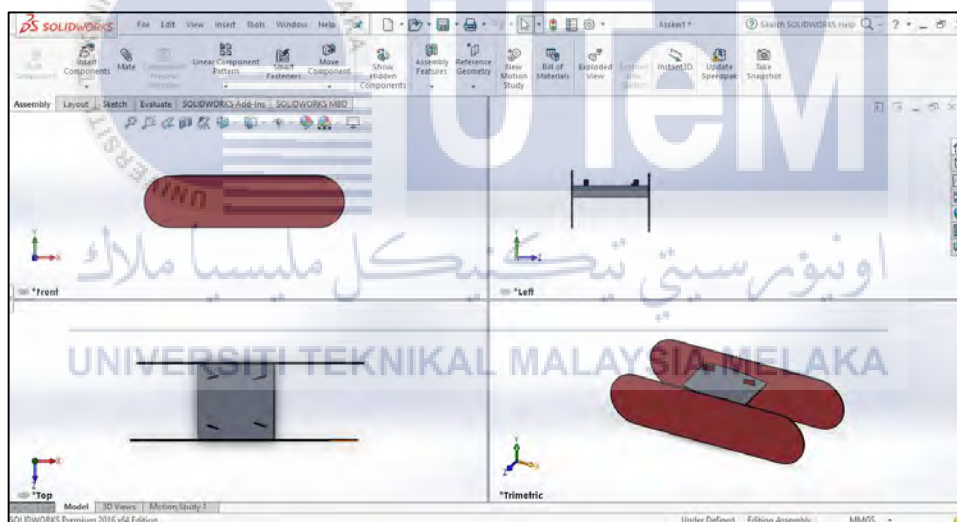


Figure 3.18: 3D Views of the Experimental Assembly (Rectangular)

Figure 3.17 and 3.18 shows the assembly components for the vortex generator experiment. The aerofoil fixed in-between the side plates. Vortex generator vanes is mounted 2 cm from leading and 2 cm away from the trailing edge and fixed with 60 and 120 degree of angles.

3.4.2 Design Explanation/Theory

When considering fluid flow through a submerged object, the object will be surrounded by the fluid and this type of flow is known as external flow. The external flow of air is particularly referred to as ‘Aerodynamics’. In the study of this type of fluid flow, the most important factor to be considered is the force creating by the flow of fluid that acts upon the object known as fluid force which consists of lift and drag forces.

3.4.2.1 Principle of Lift and Drag

Figure below indicates the forces acting on a body totally immersed in a relatively large expanse of flowing fluid. Let V be the constant, undisturbed velocity certain distance ahead of the body at static position. The fluid exerts a resultant force on the body, it is common practice to solve this resultant force into two components. One component along the line V is called resistance or drag while another component, at right angle to V , is called lift.

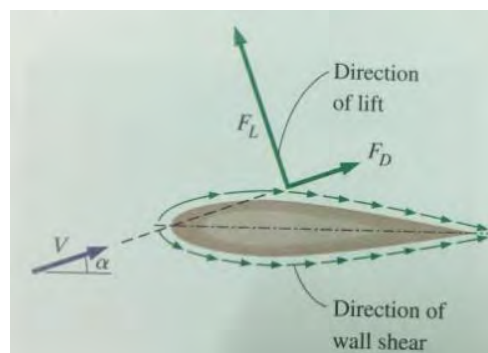
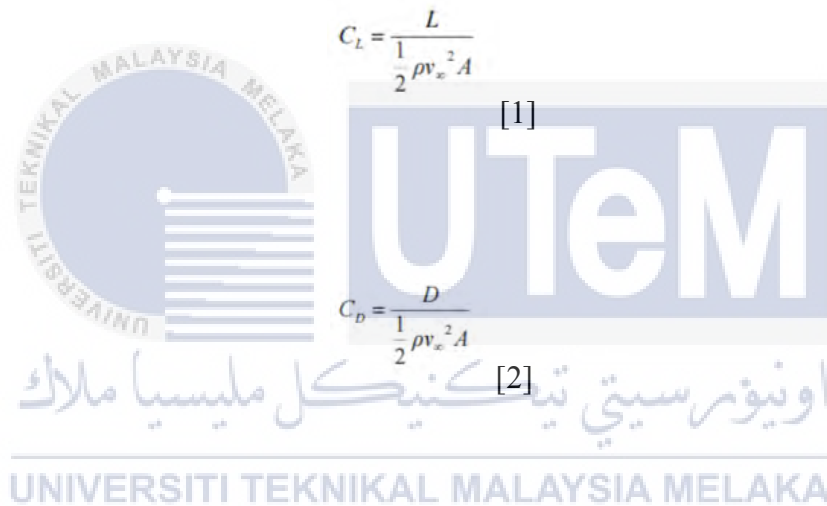


Figure 3.19: Drag and Lift Forces. (Yunus A.Cengel and John M.Cimbala, 2014)

The force applied by a fluid on a body is influenced only on the relative velocity between body and fluid while not on the absolute velocity of either fluid or body. Figure 3.19 indicates one way of gaining a definite relative motion. The similar relative motion can be recognized if the body were moving with the constant velocity V through a mass of fluid at static condition with certain distance away from the body.

Usually, lift and drag is measured in term of variable dimensionless index called lift coefficient (C_L) and drag coefficient (C_D) which can be expressed by the following formula:



$$C_L = \frac{L}{\frac{1}{2} \rho v_x^2 A} \quad [1]$$

$$C_D = \frac{D}{\frac{1}{2} \rho v_x^2 A} \quad [2]$$

Where A = Characteristic area of the object which is normally a projected area drawn around the peripheral profile of the end at the plane perpendicular to the direction of airflow.

V = Upstream wind velocity.

ρ = Density of air.

3.5 Experimental Configuration (Measurement of Lift and Drag Force)

3.5.1 Equipment Set-up

- a) Install the force measurement device supporting base plat under the test section by set the threaded hole for mounting the model's holding rod in the same corresponding vertical line of hole at the bottom of the test section and the setting of 0 degree plane of the force measurement device base plat against the direction of airflow of the test section.
- b) Insert the model holding rod through the hole below the test section and fasten the rod into the threaded hole of the force measuring device base by directing the indicator to 0 degree.
- c) Fix the model to the top of the holding rod by setting the front side of the model towards the front of the test section and fix the model onto the holding rod at this point by fastening the nut tightly.
- d) Check and verify that the model is square with the direction of air speed i.e. angle of attack is '0' by observing the centre line of the model from the top of the test section.
- e) For modify case just mount the vortex generator on the leading and trailing edge of the aerofoil with distance of 2 cm from leading and trailing edge and with 60 and 120 degree angle of tilt.

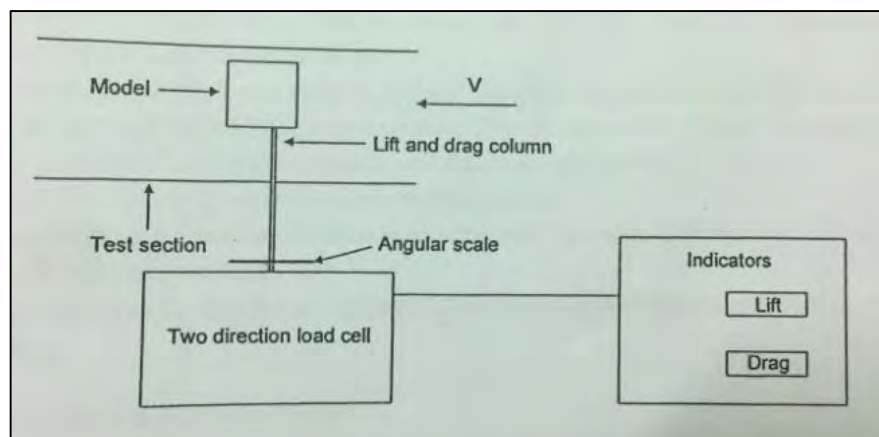


Figure 3.20: Measurement of drag and lift forces against angle of attack at various wind velocity.

3.5.2 Procedure of Experiment

- Link the drag and lift force monitor screen to the force measuring device. Check whether the reading on the screen is 0, if not 0, then record the initial values on the data sheet.
- Turn on the fan motor and alter the rotation speed till the required air velocity is achieved by checking from the measurement of the inclined manometer against the calibrated velocity graph.
- Record the values of drag force and lift force.
- Loosen the bolt/nut for locking the model holding rod to the force measurement device plat and turn the model in step of 5 degrees from 0 degree position and lock the position definitely by tightening the same bolt/nut. Record the drag and lift force.
- Repeat d for each step of 5 degree until the angle of incidence (attack) on the model is at 20 degree position at which the lift force start to decrease.

- f) Repeat step b to e for the modify case (mount the vortex generator).
- g) Plot graphs showing drag force and lift force comparing with the angle of incidence of the testing model.
- h) Calculate lift Coefficient C_L and drag coefficient C_D per data sheet and the plot graph of C_L and C_D and angle of attacks.

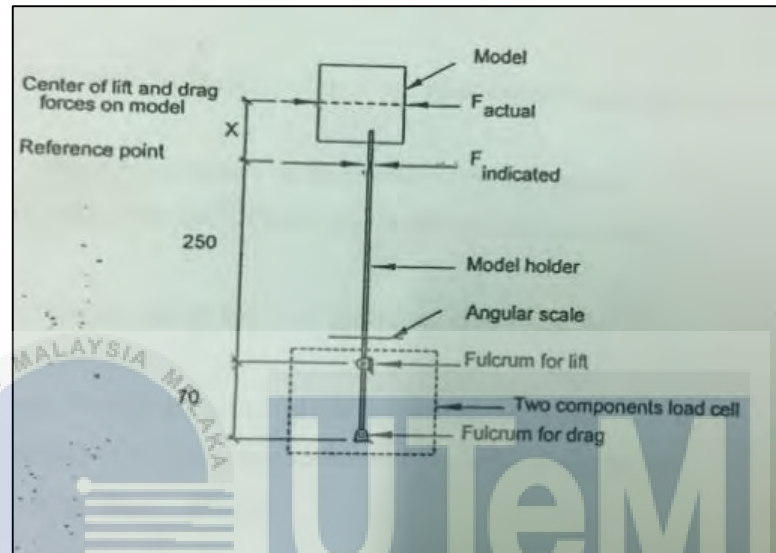


Figure 3.21: Procedure for Testing Lift and Drag Force.



Figure 3.22: Experiment Setup for Baseline Case.

CHAPTER 4

RESULTS ANALYSIS & DISCUSSION



4.1 Introduction

اونيورسيتي تيكنيكل مليسيا ملاك
UNIVERSITI TEKNIKAL MALAYSIA MELAKA

In this chapter, experimenting results of C_L and C_D are presented. The obtained results are the numerical measurement of aerodynamic performance, which allows documentation of the lift and drag coefficient. The trends of the graph can be observed and relate the condition with the principle of fluid mechanics. The effects of vortex generator can be examined through the relationship between angle of attack and C_L/C_D value.

Besides that, the position of leading and trailing edge of the NACA 0015 aerofoil are also been examined. The vortex generators are mounted on the surface of the aerofoil with specific amount of angle tilt to produce counter rotating flow.

Additionally, data recorded will be compared and determined based on aerodynamics performance. Prediction towards the aerodynamics performance is based on the C_L and C_D obtained from the experimental data.

4.2 Drag Coefficients

Normally, drag force, D indicated by:

$$D = C_D \rho \frac{v^2}{2} A \quad - [1]$$

Which, C_D is refer to the drag coefficient, a dimensionless ratio. For the entirely occupied body condition, it can be presented by dimensional analysis and dynamic similarity that C_D is a function of Reynolds number, $N_R = \rho \frac{vd}{\mu}$. Next, Figure 4.01 till Figure 4.04 below show the plots of Drag Coefficient cases, C_D against Reynolds number for numerous basic items such as for sphere and circular disk, flat plate, and for N.A.C.A airfoil 23015 at different angle of attacks.

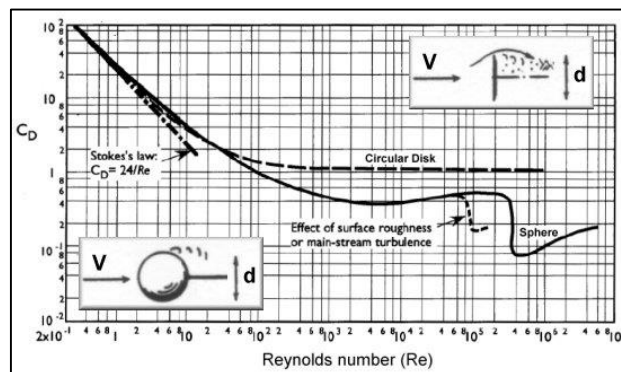


Figure 4.01: Drag Coefficients for Sphere and Circular Disk.

(<http://www.aerospaceweb.org/question/aerodynamics/q0231.shtml>)

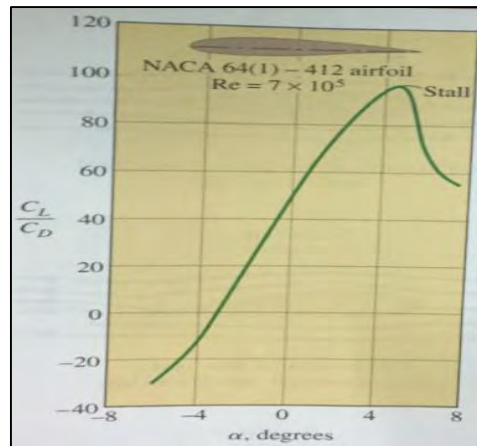


Figure 4.02: Difference of Lift to Drag Ratio with Angle of Attack for a Two Dimensional Aerofoil. (Yunus A.Cengel & John M.Cimbala, 2014)

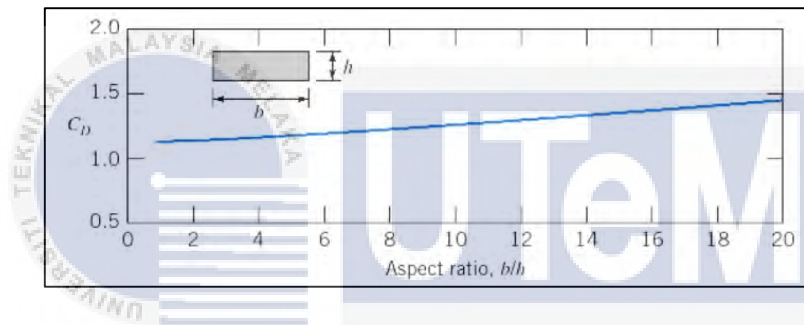


Figure 4.03: Drag Coefficients for Flat Plate of Finite Length Normal to Flow.

(<https://www.slideshare.net/manrajpal/bl-concept>)

UNIVERSITI TEKNIKAL MALAYSIA MELAKA

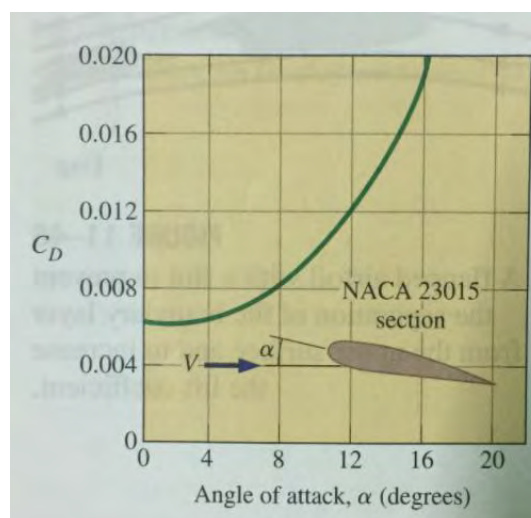


Figure 4.04: Drag Coefficient Plotted against Angle of Attack for N.A.C.A Aerofoil 23015. (Yunus A.Cengel & John M.Cimbala, 2014)

4.3 Lift Development

Figure 4.05 below indicates several agreements usually applied for discussion of vanes or section of an aerofoil. The symmetrical chord of length c is an uninformed line regularly recognized by designers in setting up the section. The angle θ concerning the chord and the line of uninterrupted velocity V is known as the angle of attack.

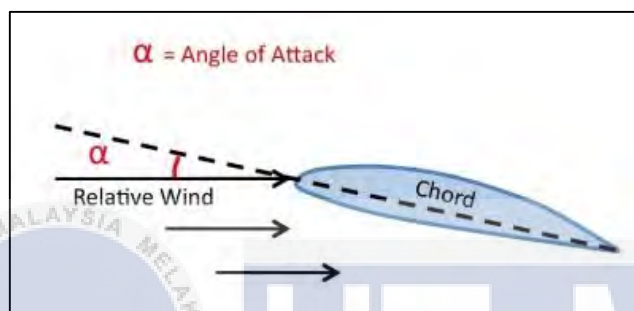


Figure 4.05: Notation of a Lifting Vane

(https://www.skybrary.aero/index.php/Angle_of_Attack)

Furthermore, Figure 4.06 next displays a diagram of the two dimensional flow throughout a vane segment positioned at an angle of attack perpendicular with the fluid flow. The streamlines were similarly move apart by specific gap during the initial point of fluid flow but then it transformed after the flow passed through the section representing the velocity different by the flowing fluid. Also included is the properties on pressure distribution throughout the section.

Let

V = velocity

p_o = pressure at some distance upstream from the section

p = pressure at any point on the vane surface

The upstream velocity or dynamic pressure is indicated by the formula of $\frac{1}{2}\rho V^2$.

It is a usual step to define pressure distribution dimension in terms of a pressure coefficient P which is a dimensionless ratio defined as:

$$P = \frac{p-p_o}{\frac{1}{2}\rho V^2} \quad - [2]$$

The upstream pressure p_o is constant. The pressure p is calculable by conducting an experiment and could be above or lower than p_o .

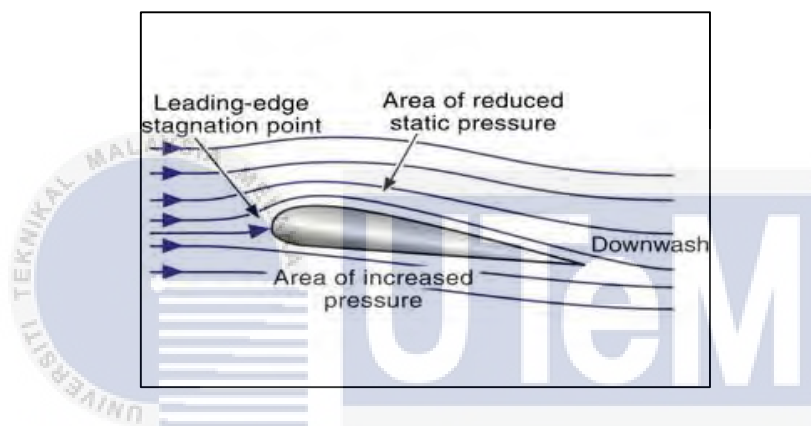


Figure 4.06: Two-dimensional Flow around a Lifting Vane

(<http://www.pilotwings.org/airfoil-pressures.html>)

Besides that, Figure 4.07 illustrated an example of pressure distribution experimental data. The pressure coefficient is plotted and gain the positive value moving downward while negative values moving upward for the change of point alongside the section surface. The net area concerning the two plotted curves, lift coefficient against chord distance in percentage of summation length is nearly proportional to the lift force due to the pressures are perpendicular to the surface and not precisely in the direction of the lift.

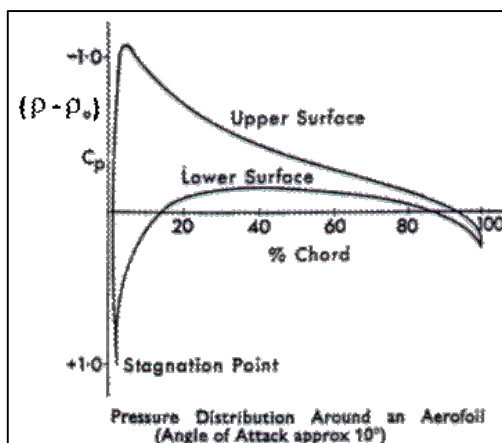


Figure 4.07: Pressure Distribution for an Aerofoil

(<http://www.scrigroup.com/limba/engleza/114/Pressure-Distribution-on-an-Ae75232.php>)

4.4 Lift Coefficients

Lift force is indicated with the following formula:

$$L = C_L \rho \frac{v^2}{2} A \quad - [3]$$

Where the lift coefficient C_L is a dimensionless. The total area A is generally recorded as the estimated area.

Numerical calculation of experimental data of lift and drag coefficients for various type of aerofoil sections can be obtained in numerous reports that have been distributed by N.A.C.A. Figure 4.08 displays an example of lift and drag coefficient against angle of attacks graph for an aerofoil. The amount of lift coefficient rises till it reaches a maximum point then it drops as the angle of attack increases. The situation occurs is also known as stall which the condition of a lifting vane operational at an angle of attack is greater compare to

the angle of attack of maximum lift. At the stall point, the working fluid split up from the vane and forms a clear eddying wake or also refer to the swirling of a fluid and create turbulent. The amount of drag coefficient will rise sharply corresponding to the stall condition is occurred.

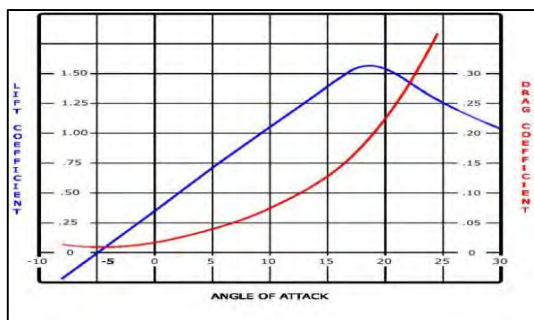


Figure 4.08: Lift and Drag Coefficients against Angle of Attacks for an Airfoil

(<http://flyacro.us/spintraining.html>)

4.5 Boundary Layer

For this case of study, the stall effect is due to the transition of boundary layer occur.

Hence, it affect the aerodynamics performance of aerofoil.

4.5.1 Boundary Layer

After a working fluid is passing through a flat plate, particles of air on the surface will cohere to the flat plate. Air particles which further apart from the flat plate will begin to

move and velocity will steadily increase with distance from the flat plate. These is when both the laminar and turbulent boundary layers occur. At the beginning, the boundary layer occurs is laminar flow with nearly linear velocity profile, causing by the viscosity of the fluid. The laminar boundary layer may possibly turn into turbulent flow when a certain distance of flow path. The equation driven for this is the Reynolds number Re is;

$$Re = \frac{Vx}{\nu} \quad - [4]$$

Where

Re = Reynold member

V = Maximum air velocity (turbulent)

ν = Dynamic viscosity of the fluid

Usual air velocities at boundary is shown in Figure 4.09 below.

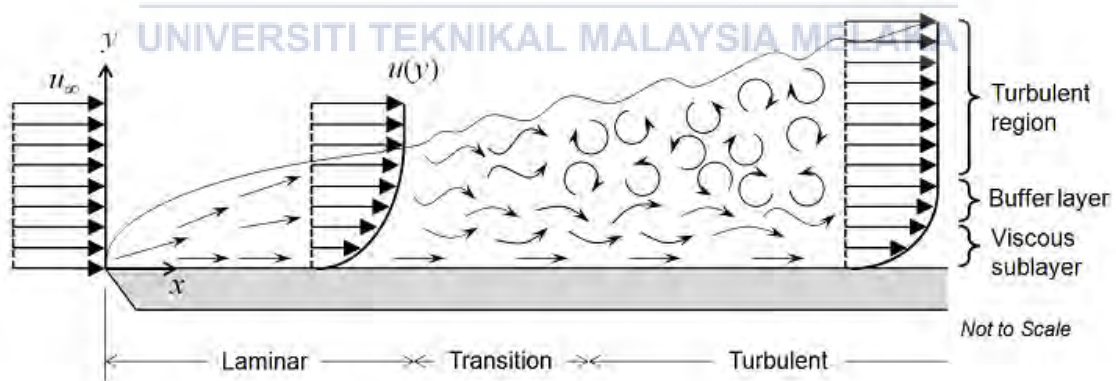


Figure 4.09: Air Velocity at Boundary. (<https://www.comsol.com/blogs/which-turbulence-model-should-choose-cfd-application/>)

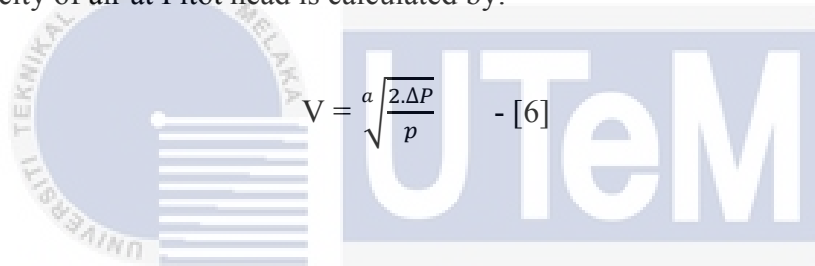
4.5.2 Air Velocity

The boundary layer thickness at the identical position reduces with the speed. The boundary layer thickness increases as the distance x from the front edge increases. The pitot tube measures the total pressure at the measuring point:

$$P_{tot} = P_{stat} + P_{dyn} \quad - [5]$$

The inclined manometer refers to the change between the total pressure and the static pressure, i.e. P_{dyn}

Velocity of air at Pitot head is calculated by:



$$V = \alpha \sqrt{\frac{2 \Delta P}{\rho}} \quad - [6]$$

$V =$ Air velocity, m/s

$\Delta P =$ Dynamic pressure or P_{dyn} , $P_a = \frac{N}{m^2}$

$\rho =$ Density of air, kg/m^3

$\alpha =$ Flow coefficient

$N = kg \times \frac{m}{s^2}$

4.6 Experimental Sample Calculation

For Aerofoil NACA 0015 aerofoil with 5 degree angle attack angle. (Baseline Case)

Data Available:

Principle Dimensions:

Cross-section Diameter Chord = 130 mm.

Width = 130 mm.

$$A = 130 \times 130 = 16,900 \text{ mm}^2$$

$$= 0.0169 \text{ m}^2$$

Indicated Drag Force (D_O) = 0.03 N, Standard distance (X_S) = 320 mm.

Actual Drag Force (D) = D N, Actual distance (X_A) = 409 mm.

$$D X_A = D_O X_S$$

$$D \times 409 = 0.03 \times 320$$

$$D = \frac{0.03 \times 320}{409} = 0.023 \text{ N}$$

Indicated Lift Force (L_O) = 0.1 N, Standard distance (X_S) = 250 mm.

Actual Lift Force (L) = L N, Actual distance (X_A) = 339 mm.

$$L X_A = L_O X_S$$

$$L \times 339 = 0.1 \times 250$$

$$L = \frac{0.1 \times 250}{339} = 0.074 \text{ N}$$

Wind Tunnel Actual Measurement;

$$\text{Drag Force } D = 0.023 \text{ N} \quad \text{Lift Force, } L = 0.074 \text{ N}$$

$$\text{Wind Velocity } V = 13 \text{ m/s} \quad \text{Air Temp, } T = 35 \text{ }^\circ\text{C}$$

Based from the air property table at the measured room temperature, the air properties are:

$$\text{At } T = 35 \text{ }^\circ\text{C}, \quad \text{Air Density } \rho = 1.146 \text{ kg/m}^3$$

Calculations for drag and lift coefficient;

Hence, from Equation 1 and Equation 2, the value of C_D and C_L can be obtain:

$$\text{Drag Coefficient, } C_D = \frac{D}{\frac{1}{2}\rho V^2 A} = \frac{0.023 \text{ kg} \frac{\text{m}}{\text{s}^2}}{\frac{1}{2} (1.146) \frac{\text{kg}}{\text{m}^3} (13^2) \frac{\text{m}^2}{\text{s}^2} (0.0169) \text{m}^2} = 0.014$$

$$\text{Lift Coefficient, } C_L = \frac{L}{\frac{1}{2}\rho V^2 A} = \frac{0.074 \text{ kg} \frac{\text{m}}{\text{s}^2}}{\frac{1}{2} (1.146) \frac{\text{kg}}{\text{m}^3} (13^2) \frac{\text{m}^2}{\text{s}^2} (0.0169) \text{m}^2} = 0.045$$

(*Note: N is equal to $\text{kg} \cdot \frac{\text{m}}{\text{s}^2}$)

4.7 Experimental Results and Analysis

- i. NACA 0015 aerofoil for baseline case with constant speed of 13 m/s:

Table 4.1: Experimental and Calculation Data to Determine C_L and C_D for Baseline Case.

| Angle of Attack (Degree) | Initial Force (IF) | | Final Force (FF) | | Indicated Force (IF) | | Actual Force (AF) | | Coefficient | | Ratio |
|-----------------------------|-----------------------|-------------|---------------------|-------------|-------------------------|-------------|----------------------|-------------|-------------|-------|-----------|
| | Lift (N) | Drag (N) | Lift (N) | Drag (N) | Lift (N) | Drag (N) | Lift (N) | Drag (N) | C_L | C_D | C_L/C_D |
| 0 | 0.00 | -0.25 | 0 | -0.22 | 0 | 0.03 | 0 | 0.023 | 0 | 0.014 | 0 |
| 5 | -0.10 | -0.29 | -0.20 | -0.23 | 0.1 | 0.06 | 0.074 | 0.047 | 0.045 | 0.029 | 1.55 |
| 10 | -0.10 | -0.33 | -0.60 | -0.20 | 0.5 | 0.13 | 0.369 | 0.102 | 0.225 | 0.062 | 3.63 |
| 15 | -0.10 | -0.33 | -0.80 | -0.19 | 0.7 | 0.14 | 0.516 | 0.110 | 0.315 | 0.067 | 4.70 |
| 17 | -0.10 | -0.33 | -0.90 | -0.18 | 0.8 | 0.15 | 0.590 | 0.117 | 0.361 | 0.071 | 5.08 |
| 18 | -0.10 | -0.33 | -1.10 | -0.17 | 1.0 | 0.16 | 0.737 | 0.125 | 0.450 | 0.076 | 5.92 |
| 19 | -0.20 | -0.34 | -1.10 | -0.15 | 0.9 | 0.19 | 0.664 | 0.149 | 0.406 | 0.091 | 4.46 |
| 20 | -0.20 | -0.34 | 1.00 | -0.12 | 0.8 | 0.22 | 0.590 | 0.172 | 0.361 | 0.105 | 3.44 |



Figure 4.10: Experimental Setup for Baseline Case.

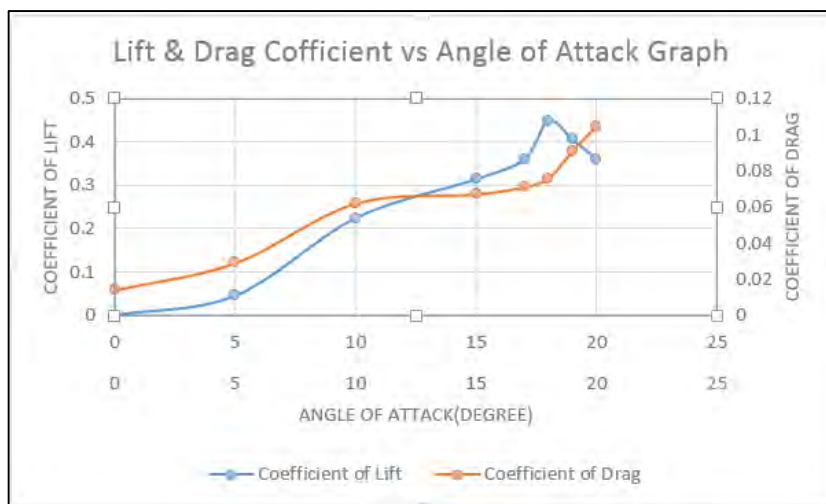


Figure 4.11: Lift and Drag Coefficient Results against Angle of Attack. (Baseline Case)

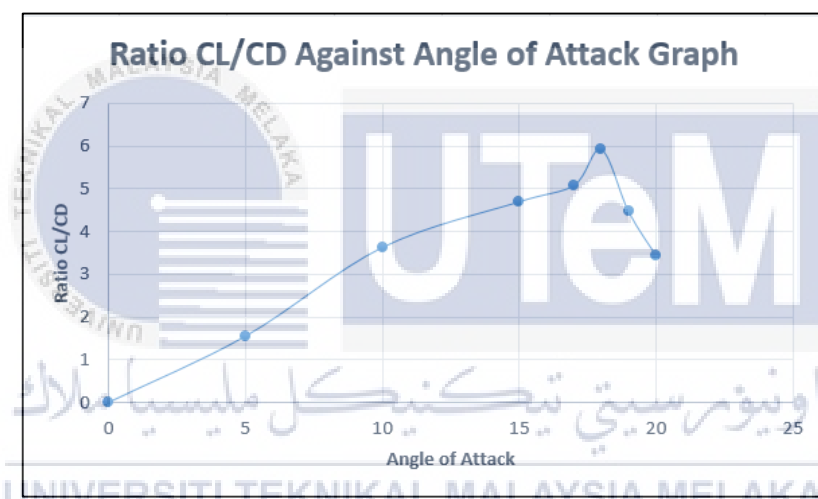


Figure 4.12: Lift and Drag Coefficient Ratio against Angle of Attack. (Baseline Case)

Table 4.1 and Figure 4.10 - 4.12 shows the results obtained by conducting vertical axis wind turbine experiment towards NACA 0015 for the baseline case condition. The velocity of fluid is set to be constant with the value of 13 m/s and air density, $\rho = 1.146 \text{ kg/m}^3$ at room temperature of 35 °C. The fixed variable is obtained from the reading of wind velocity, test section and air property table provided in Turbo Machinery Lab. The fixed variables is used for both baseline and modify case for the experiment purpose with the same surface area of NACA 0015, 13 mm x 13 mm.

From the result obtained, it shows that the amount of lift is increase steadily until it reach the critical angle of attack ($\alpha = 18^\circ$) and the aerofoil start to undergoes stall condition at C_L value of 0.450. Then, the lift coefficient decrease drastically with angle of attack, α until it reaches the maximum angle of attack applied, 20° with the amount C_L , 0.361 N. At zero angle of attack ($\alpha = 0^\circ$), the lift coefficient is zero for symmetrical NACA 0015 aerofoils. Thus in real life situation, aircrafts with symmetrical aerofoil segments need to fly using their greater angles of attack in demand to generate equal lift and overcome drag.

By referring the C_D trend line, it show the highest amount of drag coefficient value, 0.105 N at the angle of attack, 20° . At the angle of 18° , there is a change of boundary layer. Wind tunnel measurement require a correction owing to wall effects (blocking walls, flow separation, buoyancy, .etc) due to the uncertainty value of drag coefficient and it supposed to result a steadily increase trend. Moreover, lift and drag coefficient ratio against angle of attack graph shows the peak value at angle of attack, 18° and it shows the same result as shown in previous Figure 4.11. At the angle of attack 20° , drag coefficient has encounter the lift coefficient due to sudden decreased of lift coefficient. Next, the ratio of C_L/C_D decreased gradually till it reach angle of attack, 20° .

Table 4.2: Experimental and Calculation Data to Determine C_L and C_D for Modify Case.
(Rectangular VG at leading edge)

| Angle of Attack (Degree) | Initial Force (IF) | | Final Force (FF) | | Indicated Force (IF) | | Actual Force (AF) | | Coefficient | | Ratio |
|-----------------------------|-----------------------|-------------|---------------------|-------------|-------------------------|-------------|----------------------|-------------|-------------|-------|-----------|
| | Lift (N) | Drag (N) | Lift (N) | Drag (N) | Lift (N) | Drag (N) | Lift (N) | Drag (N) | C_L | C_D | C_L/C_D |
| 0 | 0.00 | -0.30 | 0.00 | -0.26 | 0 | 0.04 | 0 | 0.031 | 0 | 0.019 | 0 |
| 5 | 0.00 | -0.36 | -0.30 | -0.26 | 0.30 | 0.10 | 0.221 | 0.078 | 0.135 | 0.047 | 2.87 |
| 10 | -0.10 | -0.32 | -0.60 | -0.21 | 0.50 | 0.11 | 0.369 | 0.086 | 0.225 | 0.053 | 4.25 |
| 15 | -0.10 | -0.35 | -0.90 | -0.18 | 0.80 | 0.17 | 0.590 | 0.133 | 0.361 | 0.081 | 4.46 |
| 17 | -0.10 | -0.38 | -0.90 | -0.17 | 0.80 | 0.21 | 0.590 | 0.164 | 0.361 | 0.100 | 3.61 |
| 18 | -0.10 | -0.38 | -1.00 | -0.15 | 0.90 | 0.23 | 0.664 | 0.180 | 0.406 | 0.110 | 3.69 |
| 19 | -0.10 | -0.38 | -1.00 | -0.14 | 0.90 | 0.24 | 0.664 | 0.188 | 0.406 | 0.115 | 3.53 |
| 20 | -0.20 | -0.38 | -1.00 | -0.11 | 0.80 | 0.27 | 0.590 | 0.211 | 0.361 | 0.129 | 2.80 |

اونيورسيتي تيكنيكل مليسيا ملاك
UNIVERSITI TEKNIKAL MALAYSIA MELAKA



Figure 4.13: Experimental Setup for Modify Case. (Leading Rectangular VG)

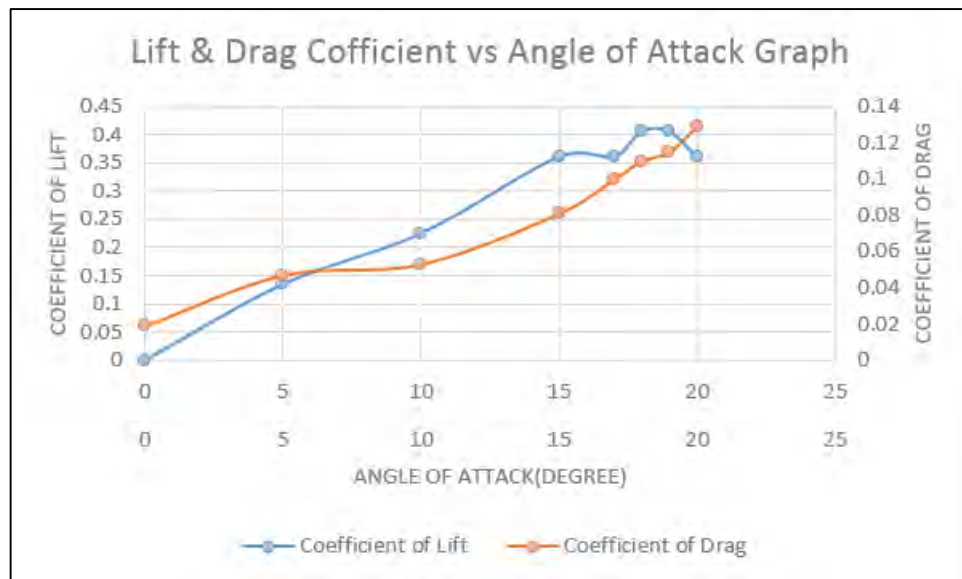


Figure 4.14: Lift and Drag Coefficient Results against Angle of Attack. (Leading Rectangular VG)

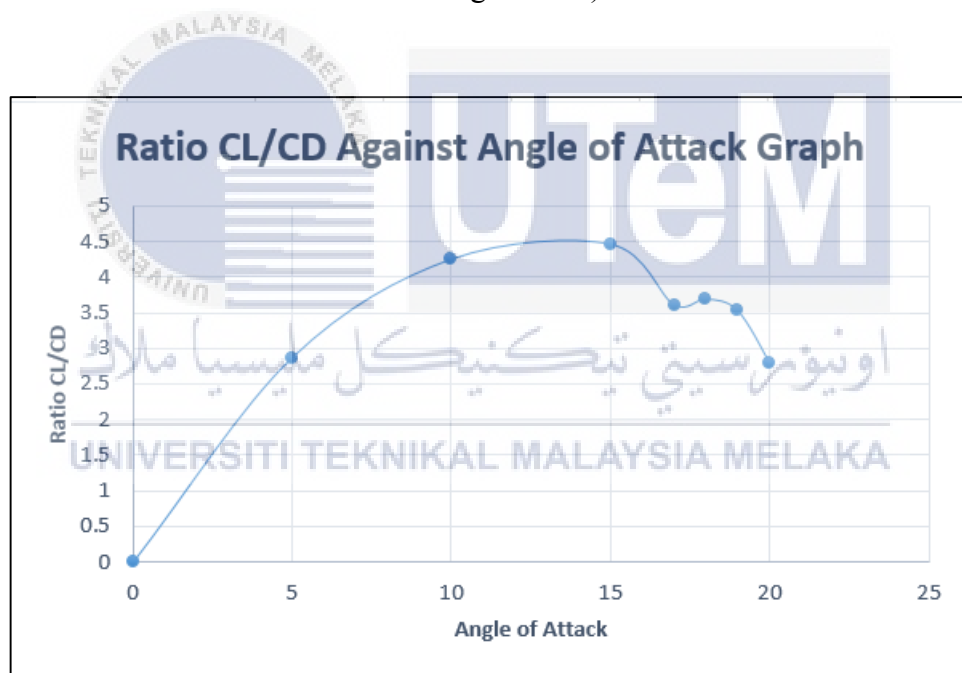


Figure 4.15: Lift and Drag Coefficient Ratio against Angle of Attack. (Leading Rectangular VG)

Next, vortex generators with a rectangular shaped is mounted on the leading edge of the aerofoil as shown in Figure 4.13. The distance of vortex generators is 2 cm away from the leading edge of the aerofoil with the angle of tilt, 60° and 120° which created a counter rotating flow.

By referring Figure 4.14, the lift coefficient rises almost linearly with angle of attack α , reaches a maximum critical angle of attack about $\alpha = 18^\circ$, and then it begins to decline suddenly. This reduction of lift with additional increase in the angle of attack is known as stall, and it is due to the flow separation and the development of a wide wake region over the top surface of the aerofoil. Stall is highly undesirable since it also increases drag.

For lift and drag coefficient ratio, it shows maximum value C_L/C_D at the angle of attack near 15° with the value of 4.46. At zero angle of attack ($\alpha = 0^\circ$), the lift coefficient is zero for symmetrical NACA 0015 aerofoils. At angle of attack ($\alpha = 20^\circ$), the value of C_D , 0.211 and recorded as the maximum.

Table 4.3: Experimental and Calculation Data to Determine C_L and C_D for Modify Case.
(Fin VG at leading edge)

| Angle of Attack (Degree) | Initial Force (IF) | | Final Force (FF) | | Indicated Force (IF) | | Actual Force (AF) | | Coefficient | | Ratio |
|--------------------------------|-----------------------|-------------|---------------------|-------------|-------------------------|-------------|----------------------|-------------|-------------|-------|-----------|
| | Lift (N) | Drag (N) | Lift (N) | Drag (N) | Lift (N) | Drag (N) | Lift (N) | Drag (N) | C_L | C_D | C_L/C_D |
| | 0 | 0.00 | -0.33 | -0.10 | -0.29 | 0.1 | 0.04 | 0.074 | 0.031 | 0.045 | 0.019 |
| 5 | 0.00 | -0.33 | -0.10 | -0.27 | 0.1 | 0.06 | 0.074 | 0.047 | 0.045 | 0.029 | 1.55 |
| 10 | -0.10 | -0.33 | -0.40 | -0.20 | 0.3 | 0.13 | 0.221 | 0.102 | 0.135 | 0.062 | 2.18 |
| 15 | -0.10 | -0.33 | -0.70 | -0.19 | 0.6 | 0.14 | 0.442 | 0.110 | 0.270 | 0.067 | 4.03 |
| 17 | -0.10 | -0.34 | -0.80 | -0.19 | 0.7 | 0.15 | 0.516 | 0.117 | 0.316 | 0.071 | 4.45 |
| 18 | -0.10 | -0.42 | -0.80 | -0.23 | 0.7 | 0.19 | 0.516 | 0.149 | 0.316 | 0.091 | 3.47 |
| 19 | -0.10 | -0.40 | -0.90 | -0.21 | 0.8 | 0.19 | 0.590 | 0.149 | 0.361 | 0.091 | 3.97 |
| 20 | -0.10 | -0.42 | -0.90 | -0.20 | 0.8 | 0.22 | 0.590 | 0.172 | 0.361 | 0.105 | 3.44 |



Figure 4.16: Experimental Setup for Modify Case. (Leading Fin VG)

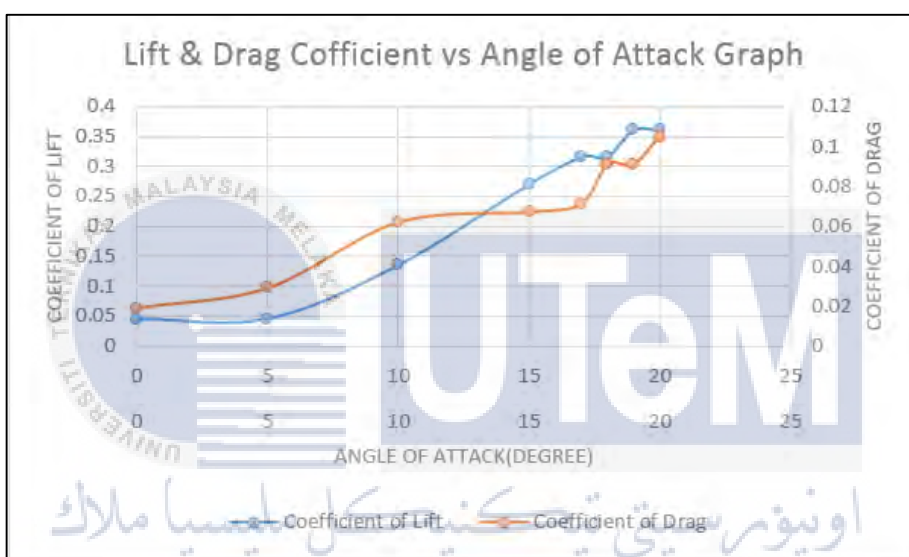


Figure 4.17: Lift and Drag Coefficient Results against Angle of Attack. (Leading Fin VG)

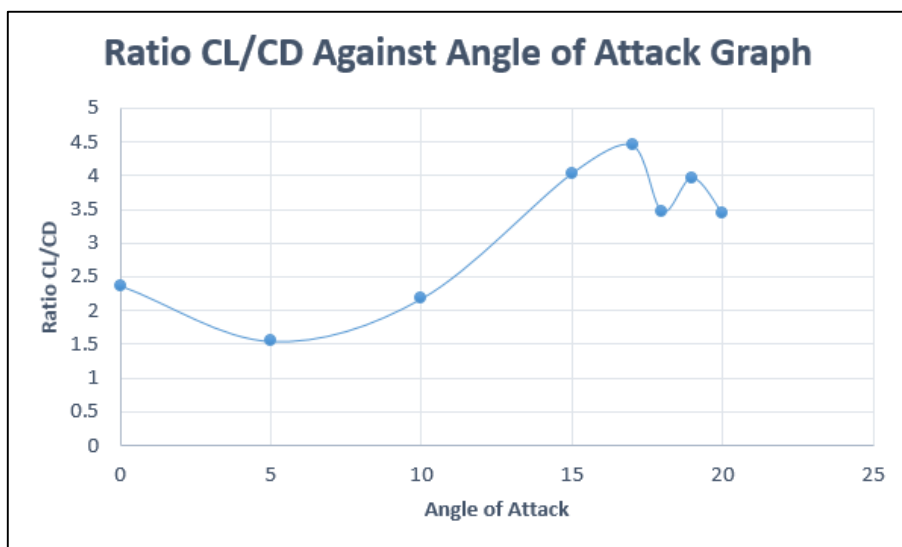


Figure 4.18: Lift and Drag Coefficient Ratio against Angle of Attack. (Leading Fin VG)

Furthermore, vortex generators with a fin shaped is mounted on the leading edge of the aerofoil as shown in Figure 4.16. The distance of vortex generators is 2 cm away from the leading edge of the aerofoil with the angle of tilt, 60° and 120° which created a counter rotating flow.

As shown in Figure 4.17, the lift coefficient show no sign of stall. Then, the amount Both C_L and C_D increments in values respectively. The amount of lift force generated by mounted vortex generator fin shaped at the leading edge shows no advance in flow separation. Also can be seen that the lift produce by baseline case, leading mounted rectangular shaped vortex generators and leading mounted fin shaped vortex generators are almost identical with the same value of $C_L=0.361$ at ($\alpha = 20^\circ$).

C_L with the highest amount recorded is 0.361 while the highest C_D recorded is 0.105. Both highest values of C_L and C_D are recorded at the angle of attack, 20° . For lift and drag coefficient ratio against angle of attacks graph, the highest amount of C_L/C_D recorded is 4.45 with the angle of attack 17° . The trend line for C_L/C_D against angle of attack graph shows fluctuating in values.

Table 4.4: Experimental and Calculation Data to Determine C_L and C_D for Modify Case.
(Rectangular VG at trailing edge)

| Angle of Attack (Degree) | Initial Force (IF) | | Final Force (FF) | | Indicated Force | | Actual Force (AF) | | Coefficient | | Ratio |
|-----------------------------|--------------------|----------|------------------|----------|-----------------|----------|-------------------|----------|-------------|-------|-----------|
| | Lift (N) | Drag (N) | Lift (N) | Drag (N) | Lift (N) | Drag (N) | Lift (N) | Drag (N) | C_L | C_D | C_L/C_D |
| 0 | 0 | -0.43 | 0 | -0.39 | 0 | 0.04 | 0 | 0.031 | 0 | 0.019 | 0 |
| 5 | -0.10 | -0.35 | -0.30 | -0.22 | 0.20 | 0.13 | 0.147 | 0.102 | 0.09 | 0.062 | 1.45 |
| 10 | -0.10 | -0.43 | -0.60 | -0.27 | 0.50 | 0.16 | 0.369 | 0.125 | 0.225 | 0.076 | 2.96 |
| 15 | -0.10 | -0.44 | -0.80 | -0.25 | 0.70 | 0.19 | 0.516 | 0.149 | 0.316 | 0.091 | 3.47 |
| 17 | +0.10 | -0.43 | -0.90 | -0.23 | 0.80 | 0.20 | 0.516 | 0.156 | 0.316 | 0.095 | 3.33 |
| 18 | -0.10 | -0.43 | -1.00 | -0.21 | 0.90 | 0.22 | 0.664 | 0.172 | 0.406 | 0.105 | 3.87 |
| 19 | -0.10 | -0.44 | -1.00 | -0.20 | 0.90 | 0.24 | 0.664 | 0.188 | 0.406 | 0.115 | 3.53 |
| 20 | -0.20 | -0.43 | -1.00 | -0.18 | 0.80 | 0.25 | 0.590 | 0.196 | 0.361 | 0.120 | 3.01 |

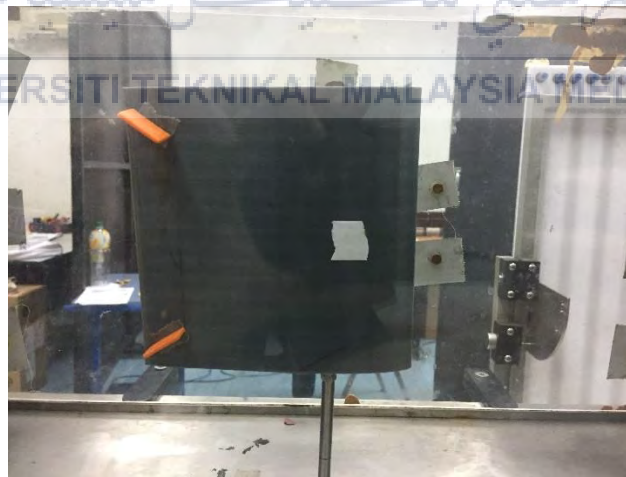


Figure 4.19: Experimental Setup for Modify Case. (Trailing Rectangular VG)

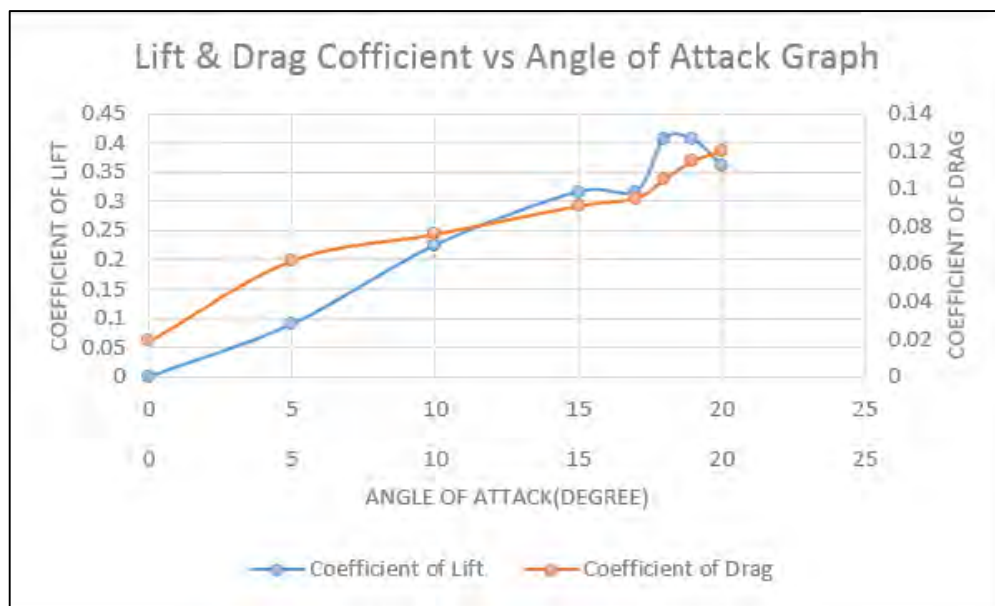


Figure 4.20: Lift and Drag Coefficient Results against Angle of Attack. (Trailing Rectangular VG)

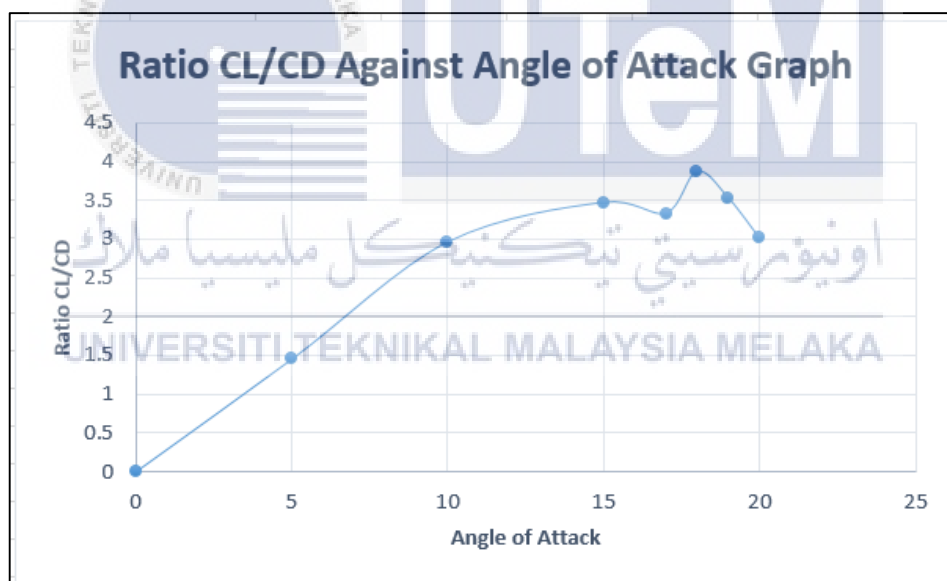


Figure 4.21: Lift and Drag Coefficient Ratio against Angle of Attack. (Trailing Rectangular VG)

Moreover, vortex generators with a rectangular shaped is mounted at the trailing edge of the aerofoil as shown in Figure 4.19. The distance of vortex generators is 2 cm away from the trailing edge of the aerofoil with the angle of tilt, 60° and 120° which created a counter rotating flow.

Next, the amount of lift coefficient is increased steadily until it reach critical angle of attack ($\alpha = 19^\circ$) with the maximum amount of $C_L=0.406$ and stall start to occurs. The amount of drag coefficient shows a steady increase trend with the maximum value of 0.120 at the angle of attack 20° . These significant amount increment of drag coefficient influence in stall condition occurred on the tested aerofoil.

While for the C_L/C_D ratio against angle of attack graph shows decrease in value starting from the angle of attack 18° with the maximum ratio value of 3.87. It started to decrease till ($\alpha = 20^\circ$) with the recorded value 3.01. This data can be clearly seen which have the similarity between the leading mounted rectangular shaped vortex generators.

Table 4.5: Experimental and Calculation Data to Determine C_L and C_D for Modify Case.
(Fin VG at trailing edge)

| Angle of Attack (Degree) | Initial Force (IF) | | Final Force (FF) | | Indicated Force | | Actual Force (AF) | | Coefficient | | Ratio |
|-----------------------------|-----------------------|-------------|---------------------|-------------|--------------------|-------------|----------------------|-------------|-------------|-------|-----------|
| | Lift (N) | Drag (N) | Lift (N) | Drag (N) | Lift (N) | Drag (N) | Lift (N) | Drag (N) | C_L | C_D | C_L/C_D |
| | 0 | 0 | -0.42 | -0.10 | -0.38 | 0.10 | 0.04 | 0.074 | 0.031 | 0.045 | 0.019 |
| 5 | -0.10 | -0.42 | -0.30 | -0.37 | 0.20 | 0.05 | 0.147 | 0.039 | 0.090 | 0.024 | 3.75 |
| 10 | -0.10 | -0.46 | -0.40 | -0.34 | 0.30 | 0.12 | 0.221 | 0.094 | 0.135 | 0.057 | 2.37 |
| 15 | -0.10 | -0.47 | -0.70 | -0.31 | 0.50 | 0.16 | 0.369 | 0.125 | 0.225 | 0.076 | 2.96 |
| 17 | -0.10 | -0.45 | -0.90 | -0.31 | 0.80 | 0.14 | 0.590 | 0.110 | 0.361 | 0.067 | 5.39 |
| 18 | -0.10 | -0.48 | -0.90 | -0.29 | 0.80 | 0.19 | 0.590 | 0.149 | 0.361 | 0.091 | 3.98 |
| 19 | -0.20 | -0.48 | -1.10 | -0.27 | 0.90 | 0.21 | 0.664 | 0.164 | 0.406 | 0.100 | 4.06 |
| 20 | -0.20 | -0.48 | -1.20 | -0.26 | 1.00 | 0.22 | 0.737 | 0.172 | 0.450 | 0.105 | 4.29 |



Figure 4.22: Experimental Setup for Modify Case. (Trailing Fin VG)

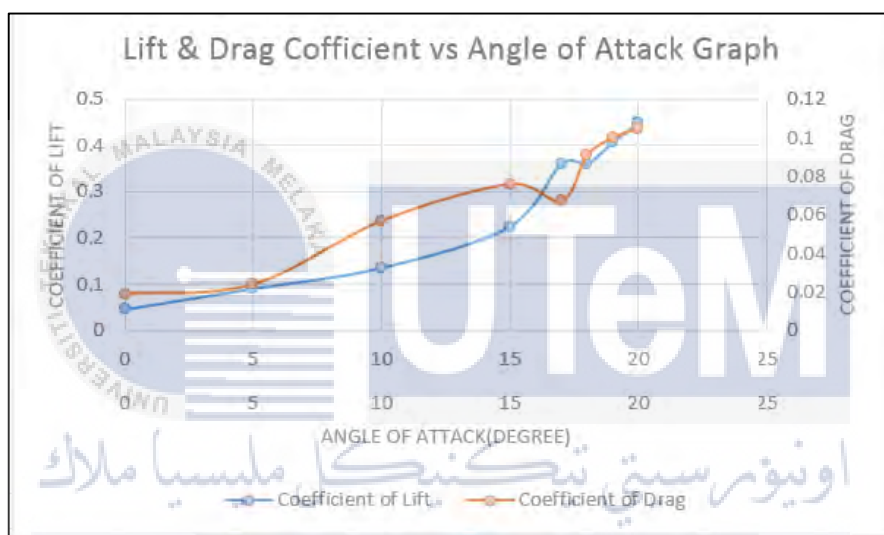


Figure 4.23: Lift and Drag Coefficient Results against Angle of Attack. (Trailing Fin VG)

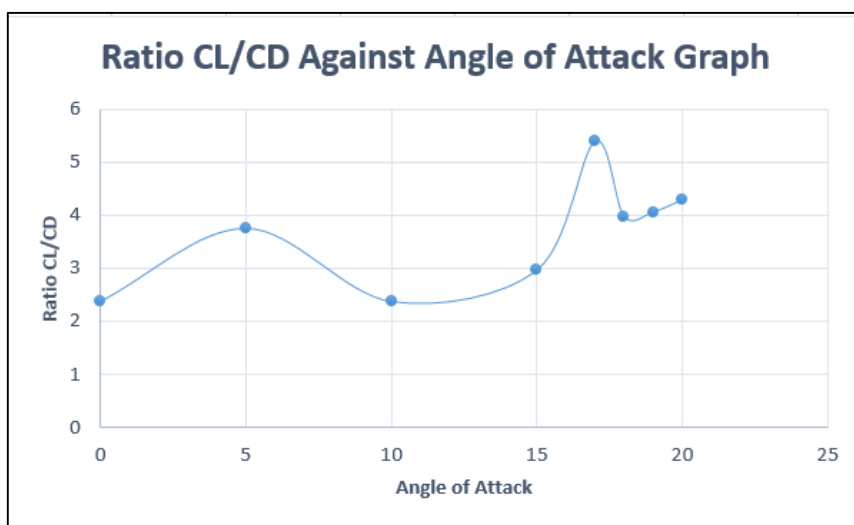


Figure 4.24: Lift and Drag Coefficient Ratio against Angle of Attack. (Trailing Fin VG)

Last but not least is the vortex generators with a fin shaped, mounted at the trailing edge of the aerofoil as shown in Figure 4.22. The distance of vortex generators is 2 cm away from the trailing edge of the aerofoil with the angle of tilt, 60° and 120° which created a counter rotating flow.

As shown in Figure 4.23, the coefficient of drag is at the maximum value of 0.105 at ($\alpha = 20^\circ$). It showed the significant lowest C_D produce at ($\alpha = 20^\circ$) compare to other cases. At angle of attack ($\alpha = 20^\circ$) also shows the highest recorded amount of lift coefficient, 0.450 compare to other cases. This data recorded match with the advantage of the implementation of vortex generator in aircraft industry which functional in delaying the flow separation from occurs.

Besides that, C_L/C_D ratio against angle of attack graph shows a fluctuating trend with the highest pick value of 5.39 and it indicates the highest aerodynamics performance value compare to other cases. As mentioned by earlier study, the function of vortex generator is to delay the flow separation occur towards the aerofoil. Hence, the amount of velocity or angle of attack must be increases to determine the maximum angle of attack which stalls occur for this specific case.

CHAPTER 5

RECOMMENDATION AND CONCLUSION



5.1 Recommendation

اونيورسيتي تيكنيكل مليسيا مالايه
UNIVERSITI TEKNIKAL MALAYSIA MELAKA

The properties of vortex generator mounted on a NACA 0015 aerofoil were investigated in a vertical axis wind turbine. The experimental study is focusing on the justification common aerodynamics performance influenced by vortex generators and the experiment aims to study the type of aerofoil being used, fix air velocity measurement ($v = 13$ m/s) and measure C_D and C_L for both baseline and modify cases besides obtains aerodynamic performance for NACA 0015 aerofoil. The collected data indicate that the aerodynamic performance of modify case aerofoil be able to develop by proper setup and optimisation of vortex generators. The amount of air velocity supplied is low with the amount of 13 m/s due to the capacity of wind tunnel. Although the wind tunnel can supply

till 30 m/s of wind, there is a problem with the power supply. To prevent any electrical circuit breakdown, the speed control module reading must be increase by five unit per session until it reach the demanding velocity and required a lot of time to wait for a session to run. Besides that, aerofoils generally function at small angles of attack, lift performance of aerofoils at that settings had better be conserved after overwhelming flow separation at large angles of attack, incorrect setting up of vortex generators could reduce the power supply of wind tunnel at certain operational cases.

Additionally, the experimental results must be compare with CFD result to obtain more appropriate and reliable outcomes. By conducting experiment, human are tend to made errors. The example of errors that tend to made are systematic errors, random errors and parallex errors. Hence, by the aid of CFD may help in supply additional data to compare between mathematical and analytical approach. Moreover, prototype and model comparison must be made. By conducting this comparison, the actual performance and efficiency of aerofoil can be obtain and relate with the real life situation. Besides, the experiment may also be test in co-rotating fluid flow generated by vortex generator to determine which rotating flow produce better lift and drag coefficient. The implementation of DBD or known as dielectric barrier discharge on the surface of aerofoil also can apply to obtain extra results relate with the aerodynamic performance efficiency. Those aspects must be consider for future work.

5.2 Conclusion

According to the results analysis, the application of vortex generators make an agreement with the improvement of aerodynamics performance for aerofoil. Based from the results comparison between baselines and modify case, only the vortex generator mounted with fin shaped showed the positive impact of the vortex generator implementation. For the condition where vortex generator mounted with rectangular shape on NACA 0015 aerofoil, the flow separation start to occur at early stage for angle of attack which below than 20° .

The working fluid flow started to separate from the surface of the aerofoil and the streamline transform from laminar to turbulent flow. This conditions produce the lowest aerodynamics performances compared to modify case of fin shaped vortex generators mounted on the trailing edge of aerofoil due the earlier stage of flow separation occurs at the edges of aerofoil which the development of vortex bursting take place. The separated flow then interrupted by the vortex generator mounted 2 cm away from the leading and trailing edge. It cause prevention of the streamline to reattach from the surface of the aerofoil and create a higher turbulent flow. This lead to increase amount of drag force and decrease the lift generated by the aerofoil.

Consequently for the vortex generator with fin shaped mounted on the leading and trailing edges of aerofoil, there is no stall phenomena occurred and showed the lowest amount of drag coefficient value. This situation possibly lead by certain variables such as insufficient amount of wind velocity apply or low range value for angle of attack. Both rectangular and fin shaped vortex generators are mounted 2 cm away from the trailing and leading edges of aerofoil. For the rectangular shaped vortex generators, it shows similar amount of lift coefficient data but recorded higher amounts of maximum drag coefficient.

For the comparison, vortex generators with rectangular shape on the leading edge produced the highest amount of drag force compare to other cases but have similar amount of lift coefficient with other cases except for the modify fin shaped cases. Besides that, leading VGs with fin and rectangular shape and trailing VGs with rectangular shape shows no significant impact on the aerodynamics performance of the aerofoil due to identical value in coefficient of lift and C_L/C_D value compared to baseline case. The experimental effect of fin shaped vortex generator to aerodynamics performance of aerofoil indicate the highest performance for this case of study. This is due to the aerodynamic shape influence of fin shaped vortex generator which generate higher lift and undergoes lower drag forces.

Fin shaped vortex generators helps in delayed the flow separation occurs along the aerofoil effectively and maintained the boundary layer. It maintained the laminar flow attached with the upper surface of the aerofoil and produce lower drag force. For normal baseline case, as the angle of attack of NACA 0015 aerofoil increases, separation of the airflow from the upper surface of the aerofoil turn out to be extra definite, causing to a decrease in the amount of rise of the lift coefficient and produce higher drag coefficient. When the lift coefficient value start to drop at the critical angle, stall occurs and lower the aerodynamics performance of the aerofoil.

For the conclusion, the experimental study on the effect of vortex generator to aerodynamics performance of aerofoil had been obtained. The amount of C_L and C_D for baseline and modify cases have been compared and overly shows a positive impact of vortex generator. Unfortunately, for the fin shaped vortex generator cases, the C_L/C_D ratio against angle of attack graph shows a fluctuating trend in value. Improvements must be make in the future research to make an adjustment toward the manipulated variables for positive results of responding variables. Overall for this thesis, it has achieved the objective to obtain and compare the C_L and C_D values for all the different cases conducted during the experiment.

REFERENCES

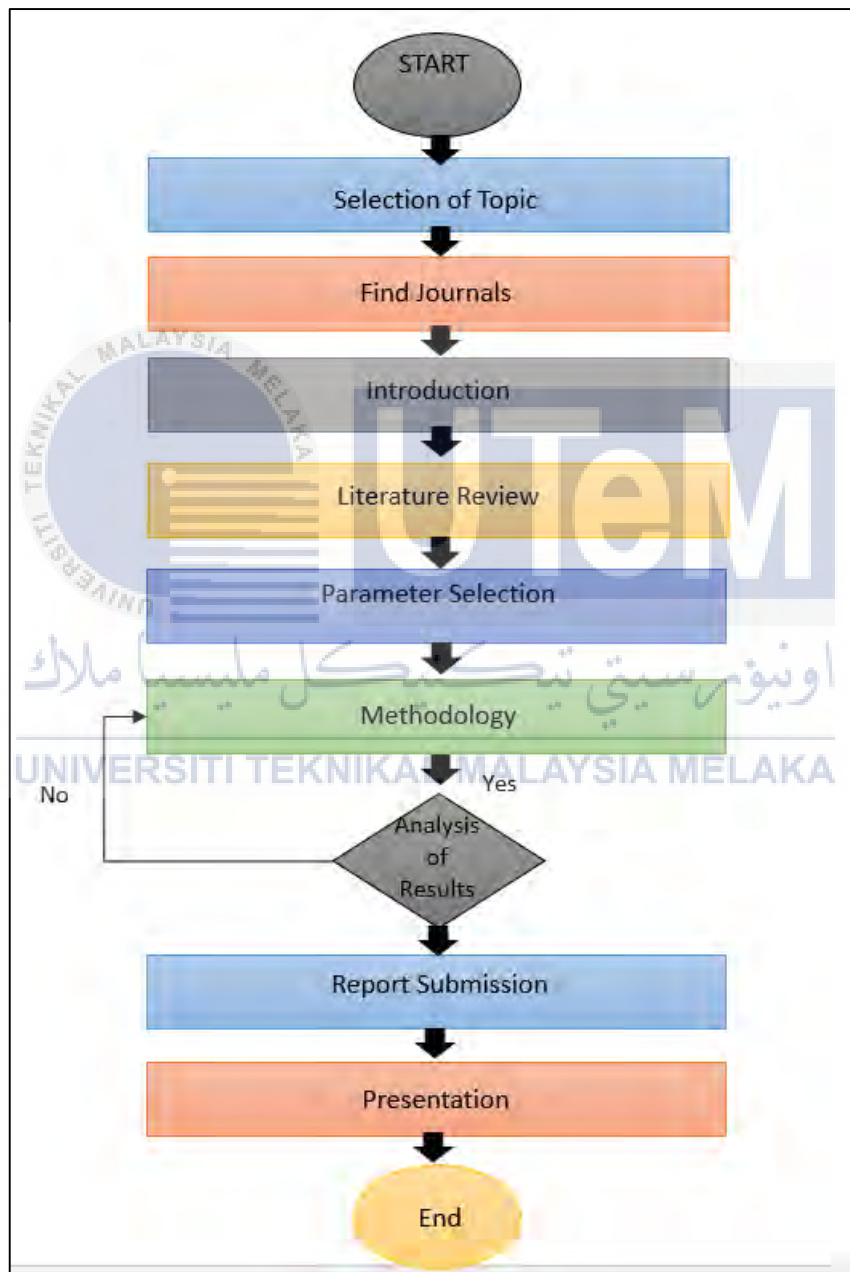
1. Allan BG, Yao C-S, Lin JC. Numerical simulation of vortex generator vanes and jets. AIAA Paper 2002-3160, 1st AIAA Flow Control Conference, St. Louis, MO, June 24–27, 2002.
2. Aman Sharma (July 2012) Evaluation of Flow Behavior around an Airfoil Body, India: Department of Mechanical Engineering Thapar University.
3. Ashill PR, Fulker JL, Hackett, KC. Research at DERA on sub boundary layer vortex generators (SBVGs). AIAA Paper 2001-0887, 39th AIAA Aerospace Sciences Meeting and Exhibit, Reno, NV, January 8–11, 2001.
4. C M Velte, M O L Hansen and D Cavar (24 January 2008) Flow analysis of vortex generators on wing sections by stereoscopic particle image velocimetry measurements, Environmental Research Letters, Volume 3, Number 1 edn., Australia: IOP Publishing Ltd.
5. Corten, G.P., 'Flow separation on Wind Turbine Blades', PhD thesis, www.library.uu.nl/digiarchief/dip/diss/1950226/inhoud.htm, univ. Utrecht, 2001

6. D. H. Thompson (February 1997) Effect of the Leading-Edge Extension (LEX) Fence on the Vortex Structure over the F/ A-18 , Air Operations Division Aeronautical and Maritime Research Laboratory edn., Australia: DSTO Aeronautical and Maritime Research Laboratory.
7. Dr. J. M. Meyers, Dr. D. G. Fletcher and Dr. Y. Dubief, 2013 (2013) Lift and Drag of an Airfoil , : MAE 123 : Mechanical Engineering Laboratory II – Fluids
8. G Godard, M Stanislas Control of a decelerating boundary layer. Part 1: optimization of passive vortex generators Aerospace Science and Technology, 10 (3) (2006), pp. 181-191
9. Gregory, N., et al., On the Stability of Three-Dimensional Boundary Layers with Application to the Flow Due to a Rotating Disk, Phil. Trans. R. Soc. Lond. A 248, (1955), 943, pp. 155-199
10. Gregory N, Quincey V, O'Reilly C, Hall D (1971) Progress report on observations of three-dimensional flow patterns obtained during stall development on aerofoils, and on the problem of measuring two-dimensional characteristics, British a.r.c.c.p
11. Hersh A, Soderman P, Hayden R. Investigation of acoustic effects of leading-edge serrations on airfoils. J Aircr. 1974; 11:197–202.
12. Ho-Joon Shim, Ki-Jung Kwon, and Seung-O Park (2017) Experimental Study on the Wake Characteristics of Vane-Type Vortex Generators in a Flat Plate Turbulent Boundary Layer , Aerospace Engineering Korea Advanced Institute of Science and Technology 291 Daehak-ro, Yuseong-gu, Daejeon 305-701 edn., Republic of Korea: Recent Advances in Fluid Mechanics and Thermal Engineering.

13. İzzet Şahin and Adem Acir (1, February 2015) Numerical and Experimental Investigations of Lift and Drag Performances of NACA 0015 Wind Turbine Airfoil, Vol. 3, No. 1 edn., : International Journal of Materials, Mechanics and Manufacturing,.
14. John D. Anderson, Jr (1991) FUNDAMENTALS OF AERODYNAMICS , Fundamentals of aerodynamics/ John D. Anderson, Jr.-2nd ed. edn., University of Maryland: McGraw-Hill Series in Aeronautical and Aerospace Engineering.
15. Johnston, J.P., Nishi, M., 1990. Vortex generator jets ± a means for \bar{c} ow separation control. AIAA Journal 28 (6), 989±994
16. K.P. Angele, Muhammad-Klingmann (2006) PIV measurements in a weakly separating and reattaching turbulent boundary layer, Volume 25, Issue 2 pages 204-222 edn.: European Journal of Mechanics - B/Fluids.
17. Kuethe AM. Effect of streamwise vortices on wake properties associated with sound generation. J Aircr 1972; 9(10):715–9.
18. Lee, B. H.; Brown, D.; Zgela, M.; Poirel, D. (SEP 1990) Wind Tunnel Investigation and Flight Tests of Tail Buffet on the CF-18 Aircraft: NATIONAL AERONAUTICAL ESTABLISHMENT OTTAWA (ONTARIO).
19. Lin JC, Selby GV, Howard FG. Exploratory study of vortex-generating devices for turbulent flow separation control. AIAA Paper 91-0042, AIAA 29th Aerospace Sciences Meeting, Reno, NV, January 7-10, 1991.
20. Lin JC, Robinson SK, McGhee RJ, Valarezo WO. Separation control on high-lift airfoils via micro-vortex generators. J Aircr 1994; 31(6):1317–23.
21. Manolesos, M., Voutsinas, S.G., 2013. Geometrical characterization of stall cells on rectangular wings. Wind Energy 17 (9), 1301–1314.

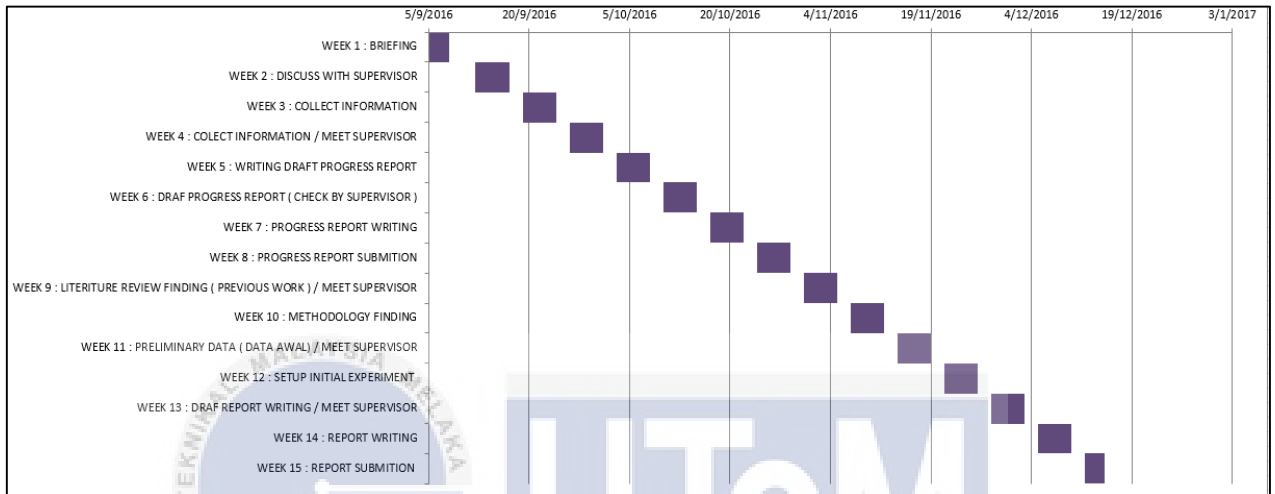
22. Manolesos M, Papadakis G, Voutsinas S (2014) Experimental and computational analysis of stall cells on rectangular wings. *J Wind Energy* 17(6):939–955
23. Manolesos M, Spyros G, Voutsinas S (28 April 2015) Experimental investigation of the flow past passive vortex generators on an airfoil experiencing three-dimensional separation, *Environmental Research Letters*, Volume 3, Number 1 edn., Greece: 2015 Elsevier Ltd.
24. Masaru Koike, Tsunehisa Nagayoshi and Naoki Hamamoto (2004) Research on Aerodynamic Drag Reduction by Vortex Generators, No. 16 edn. Mitsubishi Motors Technical Review.
25. Moss and Murdin (1971) TWO DIMENSIONAL LOW-SPEED TUNNEL TESTS ON THE N.A.C.A. 0012 SECTION INCLUDING MEASUREMENTS MADE DURING PITCHING OSCILLATIONS AT THE STALL, London: Aerodynamics Dept, R.A.E., Farnborough
26. PEARCEY, H. H., 1961. Shock-induced separation and its prevention by design and boundary layer control. In *Boundary Layer and Flow control, its principle and applications*. Vol. 2 ed. G. V. Lachmann, 1166-1344. Pergamon Press, Oxford, England. Chirokov A., Gutsol A., Fridman A., 2005, Atmospheric Pressure Plasma of Dielectric Barrier Discharges, *Pure Appl. Chem.*, Vol. 77, No. 2, pp. 487–495
27. Soderman P. Aerodynamic effects of leading-edge serrations on a two-dimensional airfoil. NASA Tech Memo. 1972;X
28. Steven D. Miller (28 MAY 2008) LIFT, DRAG AND MOMENT OF A NACA 0015 AIRFOIL, DEPARTMENT OF AEROSPACE ENGINEERING THE OHIO STATE UNIVERSITY.

29. Velte, C. M., Hansen, M. O. L. & Cavar, D. 2008 Flow analysis of vortex generators on wing sections by stereoscopic particle image velocimetry measurements. *Environ. Res. Lett.* 3, 1–11 015006.
30. Velte, C. M., & Hansen, M. O. L. (2013). Investigation of flow behind vortex generators by stereo particle image velocimetry on a thick airfoil near stall. *Wind Energy*, 16(5), 775-785. DOI: 10.1002/we.1541
31. Winkelmann AE, Barlow J (1980) Flow field model for a rectangular planform wing beyond stall. *AIAA J* 18(8):1006–1008.
32. Wokoeck, R., Krimmelbein, N., Ortman, S., Ciobaca, V., Radespiel, R., Krumbein, A.: RANS Simulations and Experiments on the Stall Behavior of an Airfoil with Laminar Separation Bubbles, AIAA-2006-0224 (2006)
33. Yao C-S, Lin JC, Allan BG. Flowfield measurement of device-induced embedded streamwise vortex on a flat plate. AIAA Paper 2002-3162, 1st AIAA Flow Control Conference, St. Louis, MO, June 24–27, 2002
34. Yon SA, Katz J (1998) Cellular structures in the flow over the flap of a two-element wing. *J Aircr* 35(2):230–232
35. Yon SA, Katz J (1998) Study of the unsteady flow features on a stalled wing. *AIAA J* 36(3):305–312
36. Yunus A.Cengel and John M.Cimbala (2014) *Fluid Mechanics*, Third Edition edn., Singapore: Mc Graw Hill
37. Zarutskaya T, Arieli R (2005) on vertical flows structures at wing stall and beyond. AIAA paper no. 4913

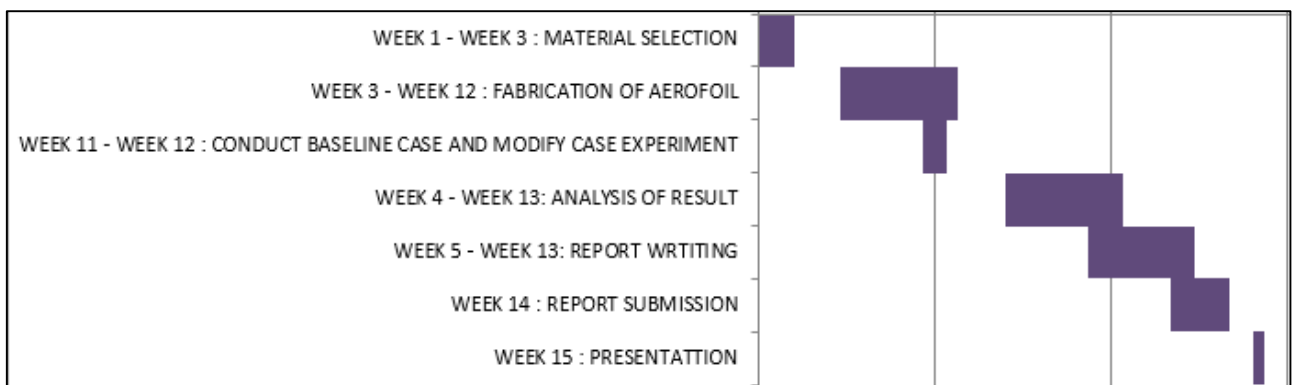
APPENDIX A: Flow Chart

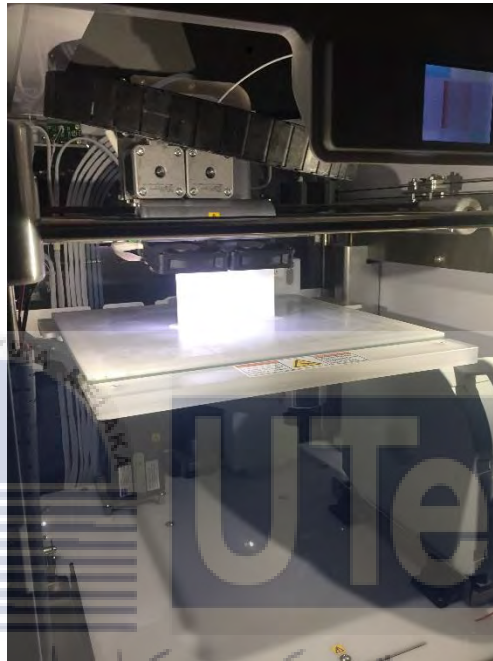
APPENDIX B: Gantt chart

FYP 1



FYP 2



APPENDIX C: 3D Printing Machine.

اونیورسیتی تکنیکل ملیسیا ملاک

UNIVERSITI TEKNIKAL MALAYSIA MELAKA

